INVESTIGATION OF A MULTI-LIGAND APPROACH TO INCREASE THERMAL STABILITY OF NBD1-ΔF508 DOMAIN OF CFTR

A thesis presented to the faculty of the Graduate School of Western Carolina University in partial fulfillment of the requirements for the degree of Master of Science in Biology

By

Christopher Shawn Robinson

Director: Dr. Robert T. Youker
Assistant Professor of Molecular Biology
Department of Biology

Committee Members: Dr. Indi Bose, Biology,
Dr. Jamie Wallen, Chemistry

November 7, 2019

ACKNOWLEDGEMENTS

I would like to thank my mother. She has always believed in my potential and encouraged me to pursue my dreams. I sincerely thank my significant other, Elizabeth Black, she has stood by me for many years and supported me in both good times and bad.

There are people at Western Carolina University I want to thank. Dr. Youker, my research advisor, for his passion and time he has given me to develop and refine my thesis. Dr. Indi Bose, committee member, a great teacher who has pushed me to critically question results and findings even from the most prestigious of sources. Dr. Jamie Wallen, committee member, for welcoming me into his lab and providing support needed to make my research possible. Dr. Lott and her research group provided me with the necessary knowledge and files for computational research. From all the countless advice and support from professors and fellow graduate students that helped me succeed throughout my time here at Western Carolina University. Finally, I would also like to thank the Phillip J. Thomas laboratory, whose donation of CFTR-NBD1-ΔF508 protein made my research possible.

TABLE OF CONTENTS

LIST OF TABLES

LIST OF FIGURES

Abstract

INVESTIGATING A MULTI-LIGAND APPROACH TO INCREASE THERMAL STABILITY OF NBD1-ΔF508 DOMAIN OF CFTR

Christopher Shawn Robinson, M.S.

Western Carolina University (November 2019)

Director: Dr. Robert Youker

Cystic Fibrosis (CF) is the most common monogenic hereditary disease in Caucasians affecting greater than 70,000 persons worldwide. Primary symptoms of CF patients are electrolyte imbalance in epithelial cells creating thick mucus layers in the lung, pancreas, and digestive track which hinders their function. The thick mucus buildup leads to CF patients having severe lung infections that eventually shorten their lifespan by decades in the most severe cases. This disease is caused by mutations in the 1480 amino acid long Cystic Fibrosis Transmembrane Conductance Regulator (CFTR) protein which regulates the chloride and bicarbonate transport across the apical membrane of epithelial cells. The most common mutation, ΔF508 in the NBD1 domain of CFTR, results in the misfolding and aggregation during protein synthesis. Such aggregates are marked for degradation preventing the protein from trafficking to the plasma membrane.

Previous screening studies have identified small corrector molecules (ligands) that can increase ΔF508 CFTR's thermal stability. These compounds enhance folding, or activity of the channel, and appear to act through binding to NBD1. Several of these compounds have been approved by the FDA to treat multiple CFTR mutations, including the ΔF508 mutation. However, the mechanism of action for these compounds is ill-defined, and there is scant information on the combinatorial effects of these compounds on the thermal stability of NBD1-ΔF508.

Purified ΔF508-NBD1 thermal stability was measured using Differential Scanning Fluorimetry (DSF) in the absence, or presence of several small molecules (BIA, Oleuropein, Hydroxy-Tyrosol) alone, or in combination. The thermal stability of ΔF508-NBD1 was increased in the presence of 1 - 5 mM ATP, as previously reported. Interestingly, lower concentrations of ATP (1.5mM) combined with 1 mM BIA had a similar effect on the stability of NBD1-ΔF508 as the higher concentration of 5 mM ATP alone. There was no change observed in the stability of NBD1-ΔF508 in the present of Oleuropein or Hydroxy-Tyrosol. Molecular dynamic simulations were performed to provide insight into the results obtained from the DSF experiments.

Introduction

Cystic Fibrosis Clinical Diagnosis

Cystic fibrosis (CF) is an autosomal recessive disease affecting approximately 70,000 individuals worldwide but appears predominantly in individuals of Caucasian descent. CF patients suffer from a variety of symptoms that affect multiple organ systems such as the pancreas, intestine, and importantly the lungs. The most commonly known symptom is chronic infection of the bronchiole tubes of the lungs. The lungs come into contact with a multitude of foreign microbial bodies such as bacteria. To prevent microbial overpopulation, mucus is secreted by the epithelial cells of the lungs to trap the microbes at the bronchi tubes. Ciliated cells sweep out the microbial trapping mucus out of the lungs into the throat to be coughed or swallowed (Baker et al. 2007). A normal individual's cystic fibrosis protein regulates the electrolyte balance of the epithelial cells that produce this mucous layer. In CF patients, the protein fails to be present in sufficient quantity to regulate the chlorine balance between the intercellular and intracellular environment. This osmotic imbalance results in an abnormally thick mucus layer that the ciliated cells are unable to move in. The end result increases the frequency and severity of lung infections which reduce the lifespan of CF patients by decades in the most severe cases (Cai et al. 2011).

CFTR protein

The Cystic fibrosis transmembrane conductance regulator (CFTR) protein is a 1480 amino acid long cAMP-regulated chloride channel with multiple domains (Schmidt, Mendoza, and Thomas 2011; Li and Naren 2011). These domains consist of two membrane spanning domains (MSD1 and MSD2), two nucleotide binding domains (NBD1 and NBD2), and a regulatory region attached to NBD1 that is responsible for controlling the gating of the channel, see Figure 1 (Hwang and Sheppard 2009). As an ABC transporter protein, this regulatory region

is unique to CFTR. The protein channel is activated by phosphorylation of the regulatory region that triggers ATP binding and heterodimeriztion of the NBD1 and NBD2 domains thus leading to channel opening (Hwang and Sheppard 2009). CFTR ΔF508 allele causes protein misfolding due to a lower thermal stability (Rabeh et al. 2012; Molinski et al. 2012; He et al. 2015). Aggregate formation occurs which eventually are marked for degradation and consequently prevents the protein from reaching its final destination at the cellular membrane (Duffieux et al. 2000; Kopito 1999).

CFTR part of the ABC Transporter Protein Family

Living creatures from the simplest prokaryotic cells to the most diverse and complex eukaryotic organisms require a means to regulate the input and output of chemical substances across the cellular membrane. This requirement led to the evolution of a large number of proteins called the ATP Binding Cassette (ABC) Transporter super-family, that evolved to break the phosphate bond in ATP to ADP as an energy source to actively move chemicals in/out of the cell through the cellular membrane. In earlier studies, it was generally accepted that this active movement was simply a “pump”, but the discovery and research of CFTR demonstrated that it can serve as a gated channel (Hwang and Sheppard 2009). The function of other ABC proteins such as multidrug resistant protein (MDR) were revised to include function of both pump and channel activities (Wilkens 2015; Vasiliou, Vasiliou, and Nebert 2008; Luckie et al. 2003).

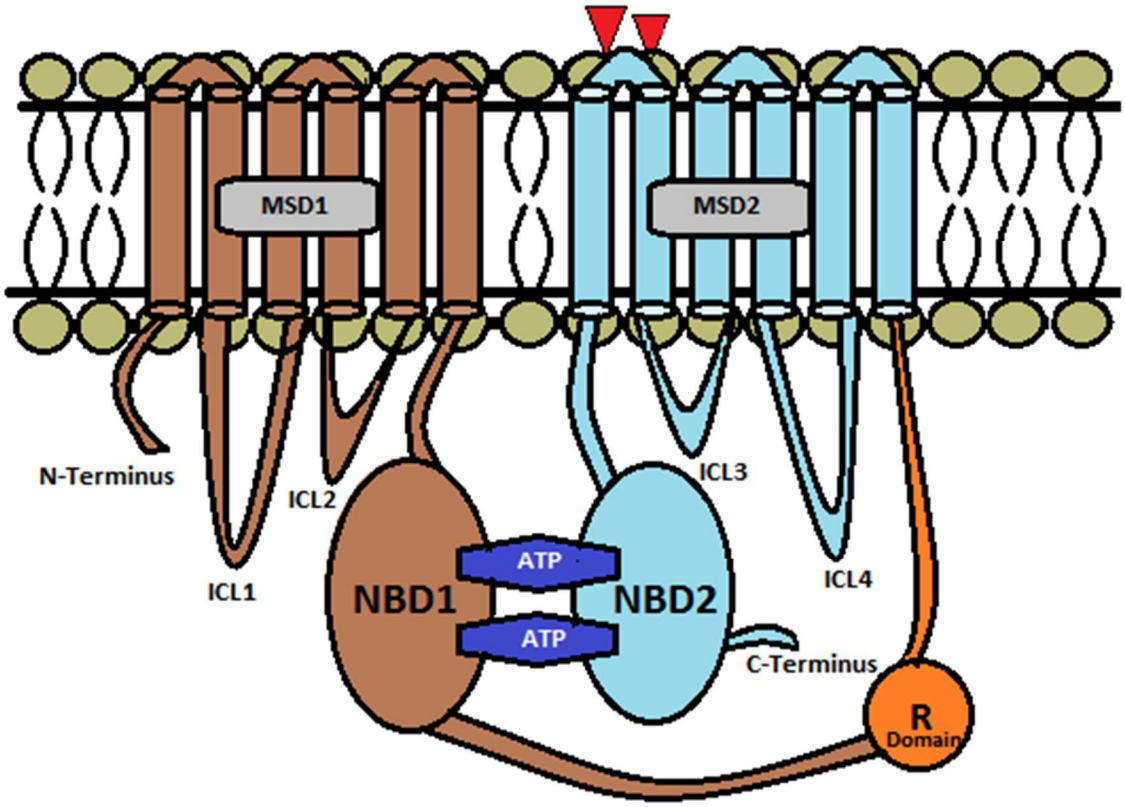

Figure 1:Illustration of CFTR structure bound to ATP.

Two glycosylation sites, illustrated as triangles, are located between helix 7 and 8 loops on residues 894 and 900.

ABC Transporter Family characteristics

The function of ABC transporters is to provide active transport of specific molecules across cellular membranes. Compared to passive diffusion, active transport requires energy in order to move molecules against a chemical gradient. This can be accomplished in two possible ways. One way is through the use of a chemical potential energy gradient by an assisting molecule. This biological mechanism is known as a secondary transport. The second way is through primary transporters which utilize the enzymatic reaction of a high potential energy molecules, such as ATP, as the mechanism the transporter protein acting as the driving force to transport polar ions or charged molecules across the cellular lipid bilayer (Vasiliou, Vasiliou, and Nebert 2008; Hwang and Sheppard 2009). Despite the different mechanisms, both types require similar structures to accomplish transport.

Proteins in the ABC superfamily have similar structures with each ABC transporter protein, including CFTR, containing two transmembrane domains (TMDs) and two nucleotide binding domains (NDBs). This protein structure could be formed by either one gene or a multiple set of genes that individual structures assemble into the final functioning unit (Biemans-Oldehinkel, Doeven, and Poolman 2006; Jones and George 2002). The TMDs are primarily hydrophobic regions that anchor the protein into the cellular membrane. Conformational changes of the TMDs allow opening for specific molecules to be transported between extracellular and intracellular areas (Patrick 2012; Hunt, Wang, and Ford 2013; ter Beek, Guskov, and Slotboom 2014; Wilkens 2015). Connected to the TMDs are the NBDs. Each NBD contain highly conserved structural motifs, Walker A (P-loop) and Walker B, that binds to an ABC family specific motif often denoted as motif C to complete the protein structure. The Walker A motif sequence, identified as GxxGxGKT (‘x’ being any residue), contains a lysine that bonds to the α-phosphate position of the ATP molecule (Hunt, Wang, and Ford 2013; Walker et al. 1982). The Walker B domain is identified by a pattern of R/KxxxGxxxLhhhDE (‘x’ denotes any

residue and ‘h’ is any hydrophobic residue)(Walker et al. 1982; Hunt, Wang, and Ford 2013; ter Beek, Guskov, and Slotboom 2014). During ATP hydrolysis, aspartate and glutamate residues of Walker B binds to Mg^{2+} and the H-motif, denoted by the conserved histidine residue, and hydrogen bonds with the γ-phosphate position of the ATP (Wilkens 2015; Biemans-Oldehinkel, Doeven, and Poolman 2006; ter Beek, Guskov, and Slotboom 2014). With Mg^{2+} and ATP bound, a glutamine residue from another structure called the Q-loop hydrogen bonds with the Mg^{2+} along with a water molecule to break the phosphate bond. The hydrolysis of ATP to ADP initiates a conformational change that rotates the NBD (Hunt, Wang, and Ford 2013). This movement is transferred by the Q-loop to the TMD allowing channeling or gating to occur depending upon the individual protein function (Jones and George 2002).

ABC Subfamily C

The ABC superfamily are divided into classes based on specialized structures and functions. Two classes are known to import chemicals while the other class exports chemical outside of the cell. While importer and exporter ABC subfamilies are both found in prokaryotes, eukaryotes almost exclusively use ABC exporter subfamilies (Wilkens 2015) . In humans, at least 49 ABC genes have been identified and organized into seven subfamilies, ABCA to ABCG, each with genes that export specific chemical substrates such as lipids, organic anions, and steroids as some examples (Dean 2001).

Most ABC subfamilies have two fully functional NBD sites but the ABCC subfamily have unique structures that differentiate it from other ABC subfamilies. The key identification of the ABCC subfamily requires a normal functioning NBD1 ATP site with the other a degenerative ATP site still capable of binding to ATP but unable to hydrolyze effectively. The NBD that contains all the functional characteristics found in other ABC proteins is called the consensus site with the nonoperating NBD denoted as the degenerative site (Wilkens 2015; ter Beek, Guskov, and Slotboom 2014). This characteristic includes only CFTR and 12 other transporters.

While CFTR is part of this family, its function as an ion channel is unique (Vasiliou, Vasiliou, and Nebert 2008; Dean 2001; Hunt, Wang, and Ford 2013).The other transporters have functions associated with multidrug resistance such as toxin excretion and signal transduction (Vasiliou, Vasiliou, and Nebert 2008).

CFTR Structure

The ABCC7 gene, CFTR, is grouped into the ABCC subfamily due to its similarities with other proteins; however, it does contain differences entirely unique from any other ABC protein. As an ABC protein, CFTR possess two TMDs and NBDs. The TMDs form the heterodimeric gating channel that allows for the movement of chloride and bicarbonate through the cellular membrane. The TMDs are described as forming “two wings” that allows for opening and closing of the gate (Patrick 2012). In the closed state, the TMDs are inward facing. Each TMD contains two alpha-helical Intracellular loops (ICLs). These ICLs have a coupling helix that forms a hydrophobic region which interact with the NBD in the cytoplasm (Zhenin, Noy, and Senderowitz 2015). ICL1 and ICL3 are known to interactive with both NBD1 and NBD2 while ICL2 solely interacts with NBD2 and ICL4 interacting with NBD1 only (Hwang and Sheppard 2009; Patrick 2012). When the ICLs of the TMDs and NBDs are properly linked, hydrolysis of an ATP molecule at the NBD heterodimeric structure causes phosphorylation of TMD-NBD1 complexes (Biemans-Oldehinkel, Doeven, and Poolman 2006; Hwang and Sheppard 2009; Baker et al. 2007). This reaction opens the TMD wings outward to allow for the chloride anion to traverse the transmembrane channel (Patrick 2012; Hunt, Wang, and Ford 2013).

In CFTR, both NBDs are divided into two subdomains called the catalytic and α-helical subdomains. The catalytic subdomain contains the conserved phosphate-binding loop Walker A and Walker B motifs along with the Q-loop and H motif (Wilkens 2015; Biemans-Oldehinkel, Doeven, and Poolman 2006; Patrick 2012; Walker et al. 1982). The α-helical subdomain motif C

is identified by the short consensus sequence “LSGGQ” found in all ABC transporters (Hunt, Wang, and Ford 2013; Biemans-Oldehinkel, Doeven, and Poolman 2006).

NBD1 of CFTR

NBD1 can be divided into three substructures. The ABC α subdomain, also known as α-helical subdomain, contains three α-helices where F508 and the ABC unique motif C is located (H.A. Lewis et al. 2010). The ABCβ subdomain contains three antiparallel β-stands and combines with the final subdomain called the ATP-binding core. The ATP-binding core is where the Walker A and B motifs are situated (H.A. Lewis et al. 2010; Patrick 2012). The ATP-binding core domain is the degeneration portion of NBD1 lacking the glutamate from Walker B motif and histidine from the H-loop used to stabilize ATP for hydrolysis.(Kidd et al. 2004; Hal A Lewis et al. 2004). The degenerative site of NBD1 contains two non-conserved regions, regulatory insert (RI) and regulatory extension (RE), located near the N-terminus and C-terminus, respectively (Patrick 2012). The R domain is found inserted between the NBD1 and TMD2 when CFTR is inactive (Baker et al. 2007; Hwang and Sheppard 2009; Zhang and Chen 2016). RI region is highly disordered which CFTR uses in regulating the gating of the channel (Hall et al. 2016; Biemans-Oldehinkel, Doeven, and Poolman 2006). This asymmetrical area at the NBD1-NBD2 interface allows for the non-phosphorylated R domain to insert itself blocking Walker A motif (Hwang and Sheppard 2009; Howell et al. 2004; Hunt, Wang, and Ford 2013). In order for the RI to initiate CFTR channel activation, multiple sites of the RI must be phosphorylated by Protein Kinase A (PKA) (Hwang and Sheppard 2009; Zhang and Chen 2016). The activation of PKA on NBD1 requires an ATP derivative called cyclic adenosine monophosphate (cAMP) to act as a secondary messenger (Molinski et al. 2012). By controlling the concentration of cAMP and PKA, the cell can control the hydrolysis of ATP at the heterodimeric NBD site.

CFTR common mutation Δ508

While there are greater than 1700 disease-causing mutations in CFTR, at least one allele containing the deletion of phenylalanine at the 508 position of CFTR is present in 90 percent of patients (H.A. Lewis et al. 2010). This in-frame deletion is located at the NBD1 site and causes surrounding residues more structural fluctuation. One structural difference is the hydrophobic V510 side chain is directly exposed to an aqueous environment in Δ508 NBD1 compared to wild type NBD1 where V510 is tightly packed to the NBD1 surface (Zhenin, Noy, and Senderowitz 2015). The deviation of the V510 residue increases misfolding rate of NBD1 portion of CFTR and ultimately causes aggregation. From previous studies, Δ508 mutation decreases the gate opening time as well as an increased exchange rate of ligand binding (Sorum, Czégé, and Csanády 2015).

Previous studies on CFTR Protein Rescue

Previous work has shown that protein stability can be compensated by various methods. The first is through low temperature treatment for protein expression to allow the protein extra time to fold during biogenesis (Sampson et al. 2011; He et al. 2015). Second, additions of chemicals that affect proteostatic regulation in the cell can help “rescue” the protein. Examples include glycerol, histone deacetylase (HDAC) inhibitors, and glafenine. Third, additional mutations have been shown to suppress certain mutations such as R553Q and G550E in ΔF508 genetic background. Finally, changes in cellular quality control systems can affect protein expression (Sampson et al. 2011). While each can help to a certain degree, they are not practical as a therapeutic method. From these findings, there have been proposals that increasing the thermal stability of the CFTR protein by a specific targeting chemical chaperone can improve folding and provide an effective rescue (Sampson et al. 2011; Schmidt, Mendoza,

and Thomas 2011). Importantly, restoring the thermal stability of NBD1 is necessary and sufficient to correct the folding and assembly defect of ΔF508 CFTR (He et al. 2015).

CFTR NBD1 Solubility and Isolation

Testing possible correctors and potentiators to stabilize the NBD1 domain has required a large expenditure of resources to overcome the many difficulties associated with isolation and purification. The first structure of NBD1 was solved by a “brute force method” of sequenced constructs that resulted in a crystal structure of the Murine NBD1 389aa-673aa and further lengthened with subsequent attempts (Hal A Lewis et al. 2004). Both short and long form are highly hydrophobic and are not easily soluble. In addition, expression of NBD1 in bacterial cultures leads to formation of inclusion bodies thus necessitating rescue/refolding paradigms to recover usable protein (Duffieux et al. 2000). To circumvent this problem, multiple solubilizing mutations such as G550R, F494N, and Q637R were created to prevent denaturation and aggregation during the isolation of CFTR D508-NBD1 (Hall et al. 2016; Molinski et al. 2012). Even with these mutations, plasmid vectors such as SUMO-Histidine tag, malotose-binding protein (MBP), and glutathione S-transferase (GST) were needed to improve NBD1 solubility during heterologous expression and purification in bacteria cultures (Hal A Lewis et al. 2004). While these epitope tags help, the yield of NBD1 is still low (0.3-0.5mg/L of culture) (Duffieux et al. 2000).

Differential Scanning Fluorimetry

The invention of differential scanning fluorimetry (DSF) method using thermal cycling machines have created a fast, inexpensive, and highly sensitive throughput process that can identify ligands which improve the thermal stability of proteins (Sampson et al. 2011). Proteins in solution tend to orient the hydrophilic regions towards the outside where they interact with water and other polar chemicals. Usually, the hydrophobic region of the protein remains on the inside

of the protein in its native state. When the temperature increases beyond a given protein stability, the protein will unfold and more hydrophobic regions are exposed (He et al. 2015; Rabeh et al. 2012; Schmidt, Mendoza, and Thomas 2011). DSF uses that phenomenon to identity thermal stability by utilizing fluorescent dye that binds to hydrophobic regions of proteins. Measuring the intensity of the fluorescence at each incremental temperature produces data that accurately identifies the protein's melting temperature that is a readout for thermal stability (Figure 2).

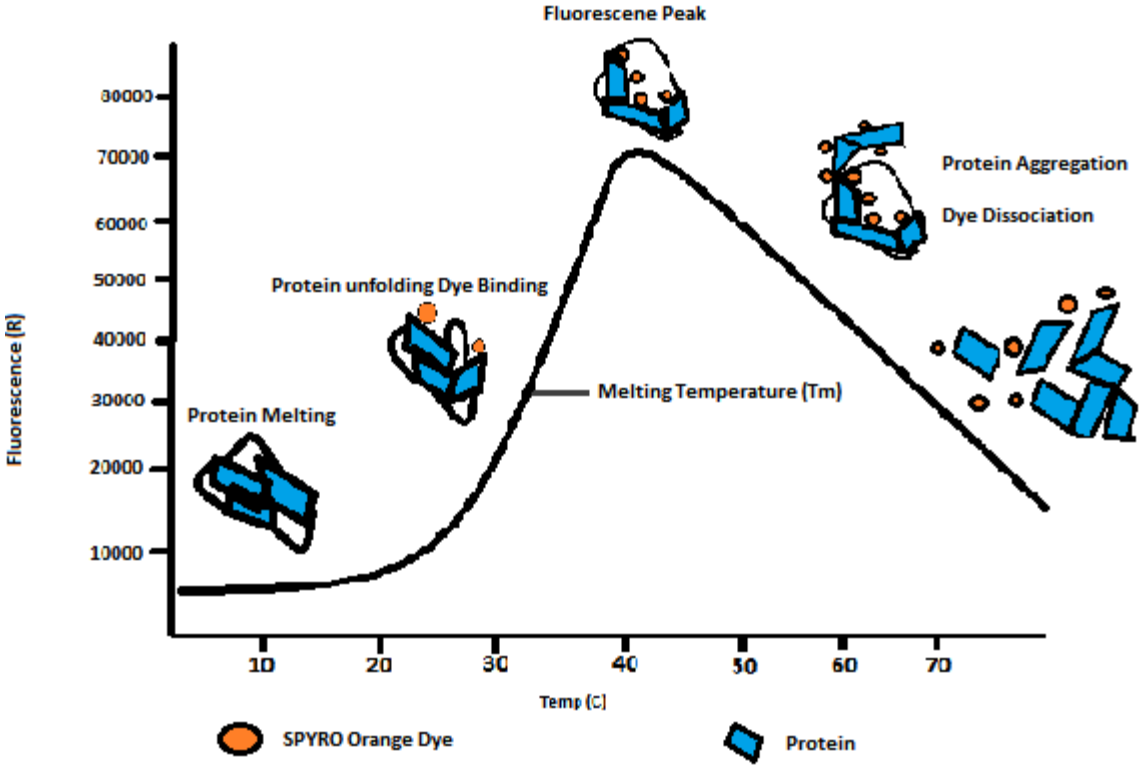

Figure 2: DSF illustration of protein unflolding and fluorescence activation by dye binding

Binding Sites of NBD1

In previous studies, CFTR NBD1 was found to have two binding sites for ligands. The first is the α-site, which is shallow in the NBD1 structure located near the a4/a5/a6 helical bundle. In a previous study, it was suggested that residue S519 is a hydrogen donor to Class A compounds which are bicyclic aromatics that possess keto or ester moiety (Hall et al. 2016). The Cp-α1 compound was predicted to affect the α-site residues of R516, S519, L594, N597, and K598 (Hall et al. 2016; Zhenin, Noy, and Senderowitz 2015). These residues were found to be distant from the NBD1-NBD2 interface and the α-site. The second site, called the β-site, is comprised of hydrophobic side chains and main-chain residues. This site was first identified with the CFFT-001 ligand molecule (Hall et al. 2016). CFFT-001 has been shown to bind and cause chemical shifts in NMR studies in the β (β_3, β_8, β_9) as well as displace α_9 helices located directly above. In another experimental study, BIA was located between the CFTR-NBD1 structural α/β subdomain and the α-subdomain. The results showed involvement with the hydrogen bond and π-cation interactions of the β-site (Hall et al. 2016). A computational study of BIA and NBD1 showed BIA interacting with the V562 residue for 76% of the length of the simulation and forming a salt bridge with residue R516 for 61% of the duration (Zhenin, Noy, and Senderowitz 2015). Lack of MD studies on NBD1 before these two studies emphasizes the need for further investigation into the α-site and β-sites

Purpose

The difficulties in obtaining sufficient quantities of CFTR-NBD1 has necessitated developing low cost and highly efficient methods of screening compounds that increase CFTR-NBD1 thermal stability. While some compounds have been found, none have the potency alone to correct the thermal instability for therapeutic purposes. The purpose of this study was to

investigate the thermal stability effect of a multi-compound approach on CFTR-NBD1 using DSF and MD.

Materials and Methods

Cell Culture Growth

Standard transformation protocol was used to transform Chloramphenicol resistant DE3-LysS BL21 codon plus with Kanamycin resistant Mouse NBD1 (DNASU CAT# MmcD00287545 in pSGX5 (His and SMT3 vector) with 5 soluble mutations (Q410E, A412V, L426S, T623S, S639D). Transformed cells were plated onto LB Agar + Kanamycin + Chloramphenicol overnight at 37^0C. Selected colony was incubated in 200 ml of Terrific Broth (TB) + Kanamycin + Chloramphenicol at 37^0C until OD600 = 0.800. TB cell culture were added to 6 L of fresh TB and incubated until OD600= 0.400. TB cell culture was induced (1mM IPTG final volume) and incubated at 16^0C overnight.

NBD1-ΔF508 Purification

Samples are kept on Ice or in the Cold Room for the following process. Cells culture were transferred into containers and centrifuged at 4,000 RPM and 4^0C for 20 minutes. Supernatant was poured off and the process was repeated until cell pellets are created from total cell culture volume. Cells were re-suspended in 10ml of lysis buffer: 50mM Tris pH 7.6, 500mM NaCl, 100 mM L-arginine, 5mM MgCl2, 4mM ATP, 2mM beta-mercaptoethanol, 12.5 % (v/v) glycerol, 20 ul of PMSF (0.1 M), 20 ul of NP40, and 20 ul of Lysozyme (100mg/ml) per 1 Liter of original cell media starting volume then incubated on ice for 60 minutes. The re-suspended cells were combined into one container and sonicated at 1 minute (constant duty at 50%) 4 times to create cell lysate. The cell lysate was centrifuged at 40,000 RPM (4^0C) for 30 minutes. The supernatant was poured into a separate container and re-centrifuge if necessary until clear in appearance. Benzonase was added to the supernatant and incubated for 30 minutes to remove nucleic acids. The supernatant was centrifuged again for 15 minutes at

10,000g and 8^0C. Immobilized metal affinity chromatography (IMAC) was performed to capture Soluble NBD1 from supernatant lysate on shaker for 1hr followed by centrifugation at 4^0C at 500 RPM for 2 minutes to settle resin. The supernatant samples were washed 3 times using Buffer W (20mM Tris, 500 mM NaCl, 20 mM imidazole, 12.5 % (v/v) glycerol, pH 7.6) for 10 minutes each on the shaker and captured. The samples were eluted using Buffer E (20mM Tris, 250 mM NaCl, 400mM imidazole, 2mM β-mercaptoethanol, 12.5 % (v/v) glycerol, pH 7.6) overnight on the shaker at 4^0C. Cleavage was performed using SUMO tag protease at 4^0C overnight. Soluble NBD1 was collected by 30,000 MWCO dialysis tubing in Buffer S (Buffer S: 50mM Tris, 150mM NaCl, 5mM MgCl2, 2mM ATP, 2mM β-mercaptoethanol, pH 7.6 and stored at -80^0C. All purification step fractions were analyzed by Western blot and electrophoresis gels to identify the presence of NBD1.

Gel Electrophoresis and Staining

The stain free gel was performed using Bio Rad protocol. The comb in the pre-cast gel was removed along with the tape. The Mini-protean tetra cell was assembled, and precast gel loaded. The Running buffer was created using 1x Laemmli SDS-PAGE by adding 100 μl 10x TGS running buffer to 900 μl of deionized water and placed in the tetra cell assembly. 10 ul of 250kD precision plus protein standard was loaded as the ladder. A master mix loading buffer was created by adding 47.5 ul of 2x Laemmli sample buffer with 2.5 ul of β-mercaptoethanol for a total of 50 ul. Test samples were prepared by adding 50 ul of individual samples into a 1.5 ml microtube. 2ul of DNASE (2 units/ul) was added to each microtube and incubated in a water bath at 37^0C for 15 minutes. Microtubes were placed in boiling water for 5 minutes for protein denaturation. 5 ul of sample and 5 ul of master mix loading buffer was added together (10 ul total) and loaded onto the gel.

Western Blot

Western blot using BioRad Trans-blot turbo. Blot was stored overnight at 4^0C in TBST. 8 ml TBST and 2.5% BSA and 6x His tag antibody (1: 1000 Dilution) was added to blot. Incubation at room temperature for 1hr on tilt shaker. Five wash steps with 10 ml TBST was done for 5 minutes each. 10 ml (TBST and 2.5%) plus (1: 10,000 Dilution) Anti-mouse HRP-conjugated antibody was added and incubated at room temperature for 30 minutes on tilt shaker. 5 wash steps with 10 ml TBST for 5 minutes followed by 7 ml total of BioRad developing reagent.

Quantification of Protein Concentration by Gel Analysis

Serial Dilution was performed starting from a 10 mg/ml BSA stock to generate BSA concentrations of 2.0 mg/ml. 1.0 mg/ml, 0.5 mg/ml, 0.2 mg/ml, and 0.1 mg/ml. The stain free gel Bio Rad protocol was used with 10 ul of each BSA concentration with 5 ul of loading dye (total 15 ul) was added. 5 ul of loading buffer was added to each NBD1 purification sample of 5 ul, 10 ul, and 15 ul and loaded onto the gel. A 250kD precision plus protein standard was loaded as the ladder. The protein concentration was determined by analysis of Gel Doc EZ Gel software.

Differential Scanning Fluorimetry (DSF)

All reactions were done either on ice or in a cold room at 4^0C. The Applied biosystems protein thermal shift protocol was used. A 40x protein thermal shift dye was prepared by combining 4 ul of 1000x Sypro Orange dye with 96 ul of nanopure water for a total of 100 ul. Master mix solutions were created by adding each component in the order listed: 25% v/v Protein thermal shift buffer, 62.5% v/v of water in addition to any protein and/or ligand, and 12.5% 40x dye. Each sample solution was pipetted up and down 10 times to homogenize components. A 20 ul volume of sample was placed into a well and was tested in triplicate. The

well plate was sealed with MicroAmp Optical Adhesive Film and spun at 1000 rpm for 1 minute at 4^0C. Well plate was stored on ice or cold room until loaded onto 7500 real-time PCR system. A Melt curve experiment type software was used with the following set up. ROX reporter selected with no quencher. All target well type assigned with no passive reference. 20 ul of reaction volume per well with continuous ramp mode was selected. Run was started with Step 1 at 25^0C with a ramp rate of 100% (1.6^0C/s) for 2 minutes. Then Step 2 at 99^0C with 1% ramp rate (0.05^0C/s).DSF results were exported to text file and analyzed by the Differential Scanning Fluorimetry Melting Data analysis tool dman2.6 to get melting point temperatures (C. K. Wang et al. 2012).

Docking of BIA and Oleuropein to NBD1-ΔF508

Missing residues were added to the 4wz6 NBD1 construct model (aa 389-678 NBD1-ΔF508 with three solubilizing mutations and bound ATP) and refined to allow for residue flexibility. Completed 4wz6 was uploaded to SwissDock for docking simulations (Grosdidier, Zoete, and Michielin 2011). Oleuropein and BIA molecule files were created in MOL2 file format by the Dr. Lott Research group. Docking simulations of 4wz6 NBD1 were performed with each individual ligand by Swissdock default settings. Swissdock used CHARMM format EADock DSS software variant that loads 5,000-15,000 binding modes and calculate the most favorable energies using the FACTS implicit solvent model (Grosdidier, Zoete, and Michielin 2011). Molecular graphics and analysis were performed with UCSF Chimera software (Pettersen et al. 2004). Ligand coordinates were removed from consideration if any exhibit any of the following: orientation of ligand away from NBD1, ligands bound to NBD1-NBD2 interface, and positive full fitness or ΔG scores. Full Fitness of a cluster was analyzed by calculating the averages of the 30% most favorable effective energies of the cluster's elements (Aurélien Grosdidier, Zoete, and Michielin 2007; Djanic et al., n.d.; Kolluru et al. 2019; Vela-Corcía et al. 2018).

NBD1 Molecular Dynamics Simulation

BIA and Oleuropein coordinates for NAMD MD simulations were selected from the docking results and merged with 4wz6 NBD to form BIA-NBD1 and Oleuropein-NBD1 PDB files. A Protein Structure File (psf) for each merged docking file was created in VMD using CHARMM force field all36 and toppar parameters (Phillips et al. 2005; Humphrey, Dalke, and Schulten 1996). Solvation box was generated for each PDB file and psf file. Periodic boundaries of the solvate boxes were calculated. A 500 step 1 ps MD minimization run at constant temperature constant pressure (npt) for each were performed. The MD of the protein-ligand in explicit solvent was heated with weak restraints on the solute with a temperature run from 0 K to 310 K using the Langevin temperature equilibrium scheme under constant volume for 50,000 MD steps. A MD equilibration of the waters and ions were implemented at constant 310 K and pressure at 1 bar for 100,000 MD simulation steps. A MD production was with constant temperature and pressure and conditions similar to the previous MD equilibrations except with 5,000,000 MD simulation steps (10ns). Root mean square fluctuations (RMSF) calculations per residue was performed.

Results

Docking of Ligands to NBD1

Molecular Dynamic simulations served as a predictor for potential binding of ligands to NBD1-ΔF508. ATP was present in the crystal structure of NBD1-ΔF508 (PDB: 4wz6) and no docking was performed for this ligand. BIA had been found to bind to NBD1 in previous *in vitro* and MD studies around the α/β-subdomains (Sampson et al. 2011; Hall et al. 2016; Zhenin, Noy, and Senderowitz 2015; He et al. 2015). Swissdock results confirmed that BIA docked between the ABCα-subdomain and ABCβ-subdomain (Figure 3a). The $BIA_{\Delta G}$ was -5.786711 a full fitness score of -1766.115 a.u (Table 1) demonstrating a possible spontaneous reaction to bind to NBD1-ΔF508.Swissdock produced an Oleuropein dock at the location where NBD1-ATP interface with NBD2 (Figure 3b). $Oleuropein_{\Delta G}$ was observed to be -7.164446 with a full fitness score of -1716.6572 kcal/mol (Table 1), although spontaneous in regards to a reaction, the Oleuropein interface did not meet the criteria for MD simulation as its docking location is in spatial conflict with the interface of NBD2 with ATP and NBD (Figure 4).

MD Simulation of NBD1-ΔF508 with BIA

MD Simulation of NBD1-ΔF508 in the presence of BIA were ran to measure root mean square fluctuations (RMSF), see Figure 5. While there were areas of greater fluctuation, the addition of BIA to NBD1 had an overall positive increased thermal stability. Specifically, the 4wz6 construct (389aa-678aa) had a minor increase in variable fluctuation from 479-487 with a maximum fluctuation at 0.42 Å, Figure 6a. Minor fluctuations occurred between residues 489-492 with residue 489 having 0.21 Å increased fluctuation, Figure 6b. The residues 509-516, which contains some α subdomain residues, increased in fluctuation with the maximum of 0.40 Å at residue 512, Figure 6c. These residues were after ΔF508 and were known for increased fluctuations in NBD1-ΔF508 when compared to wt NBD1 (Zhenin, Noy, and Senderowitz 2015).

Residues 559-571 had the greatest fluctuation with a maximum RMSF value of 0.46 Å at residue 565, Figure 6d. These residues were located in the binding site area of BIA. The first area of reduced fluctuation of note occurred in the regulatory insertion region (RI) 422-431, Figure 7a. The crystal structure for these residues did not have enough resolution to define the dimensional coordinates of the RI region (405-436) and were added to the PDB file before docking to maintain NBD1 structure integrity. The stabilization results of this area cannot be truly reported with the crystal structure 4wz6 template.(Zhenin, Noy, and Senderowitz 2015). ATP Binding Residues, 454-465, had reduced fluctuation with the addition of BIA to NBD1-ΔF508, Figure 7b. The residue that had greatest reduction in that range was residue 460 at 0.4 Å. The residue area before ΔF508, 500-507, demonstrated stabilization compared to the destabilization of residues after ΔF508 with both residue 506 and 507 reduced fluctuation at 0.34 Å each, Figure 6c and 7c,. The next stabilized residues were near BIA docking close to the α/β subdomains 517-543. The greatest reduction was 0.65 Å at residue 528, Figure 7d. Residues 602-630 had minor reduction in fluctuation with the exception of residue 619 which was reduced by 0.44 Å, Figure 7e. Another reduced fluctuation from 656-678 was noted but not important since the range includes the naturally disordered regulatory domain (Baker et al. 2007).

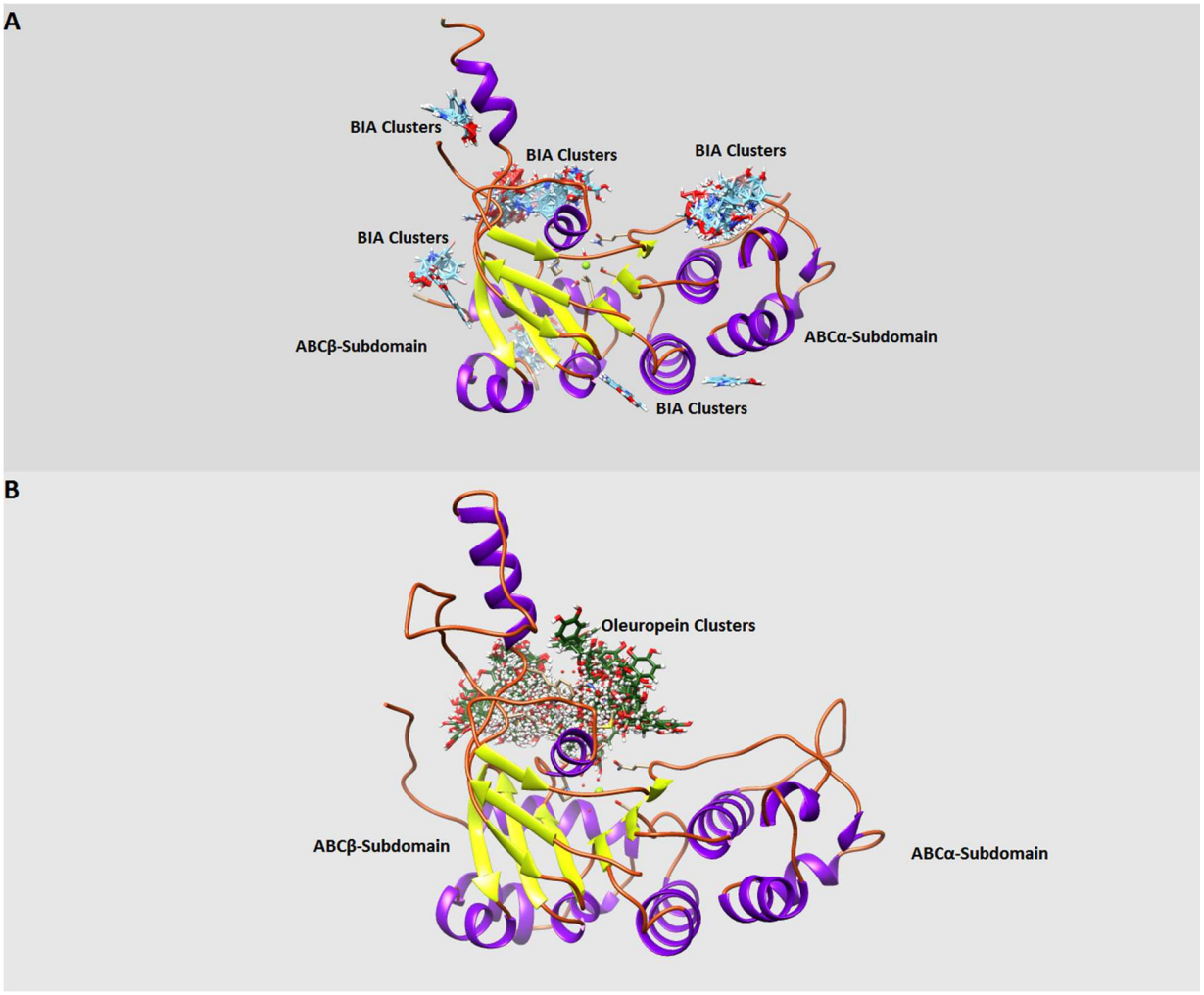

Figure 3 Full Cluster Docking Results

A) Docking clusters of BIA to NBD1. B) Docking clusters of Oleuropein to NBD1.

Name	Full Fitness kcal/mol	ΔG kcal/mol
BIA	-1766.11572	-5.786711
Oleuropein	-1716.6572	-7.164446

Table 1: Ligand-NBD1 docking scores of BIA and Oleuropein full fitness and ΔG values.

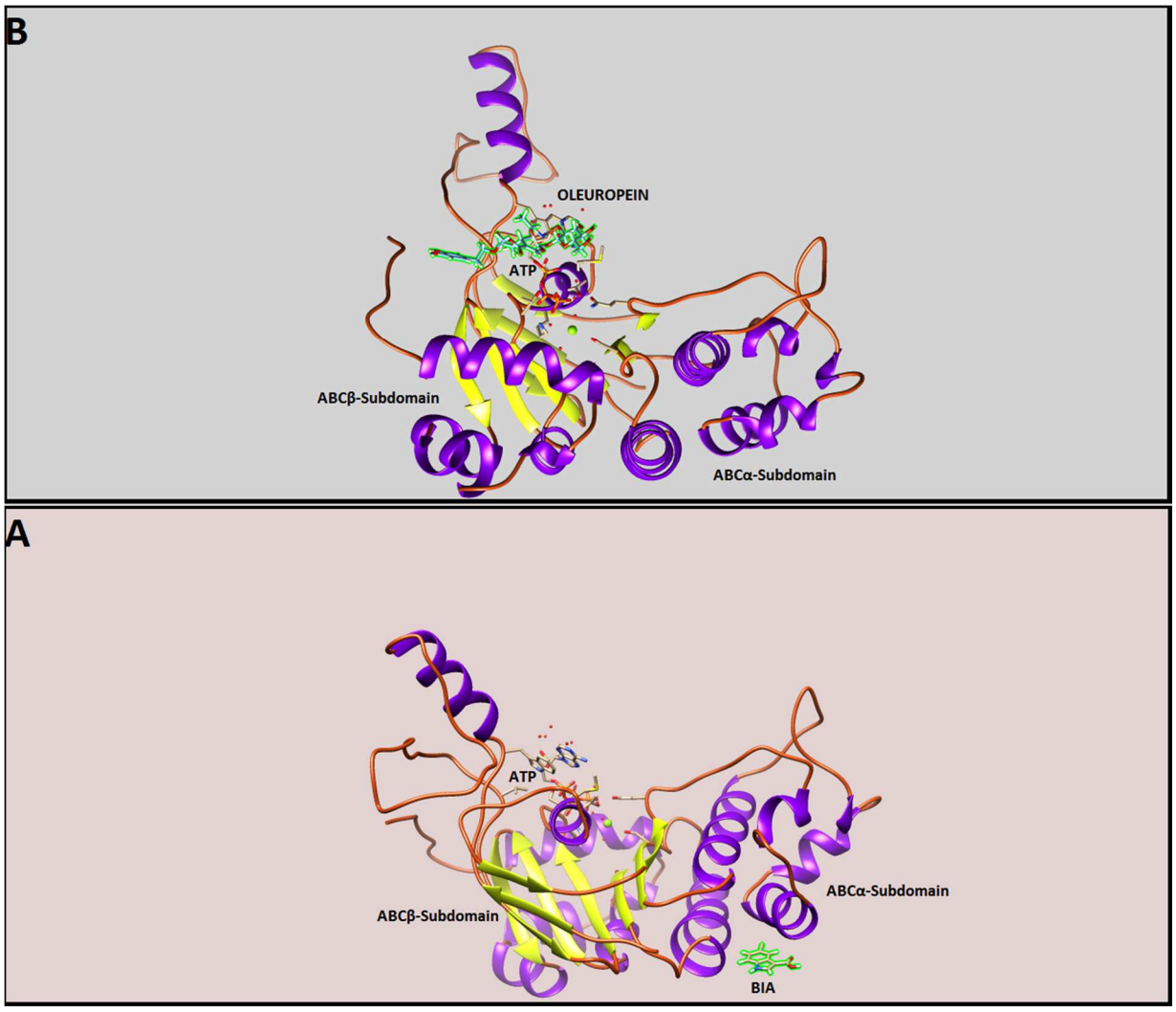

Figure 4:Ligand docking results of NBD1

A) BIA docking to NBD1. B) Oleuropein docking to NBD1 located at the NBD1-ATP-NBD2 interface.

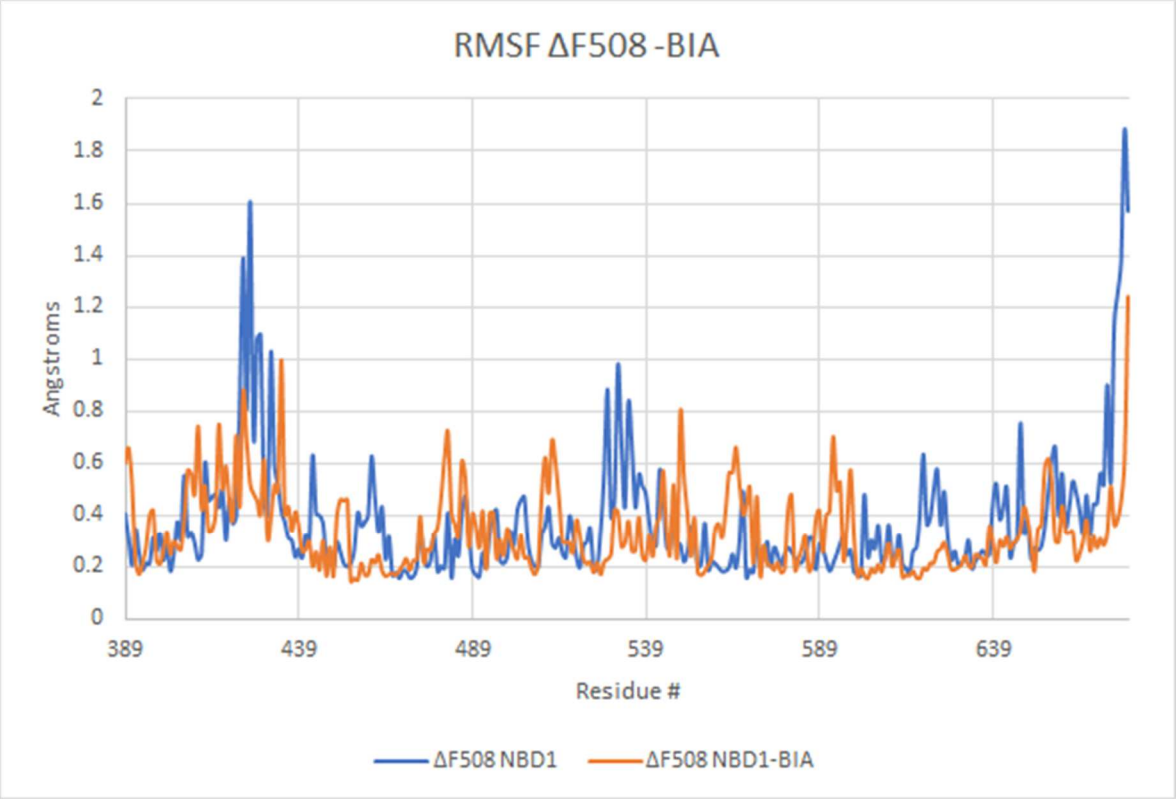

Figure 5:Average RMSF Plot per residue of NBD1-ΔF508 with/without BIA.

RMSF calculated from VMD Timeline of 10,000 frames at a 50-stride setting. RMSF raw data was exported and an average RMSF was calculated derived from the sum of absolute position fluctuation in Angstroms of each residue relative to the simulation starting position.

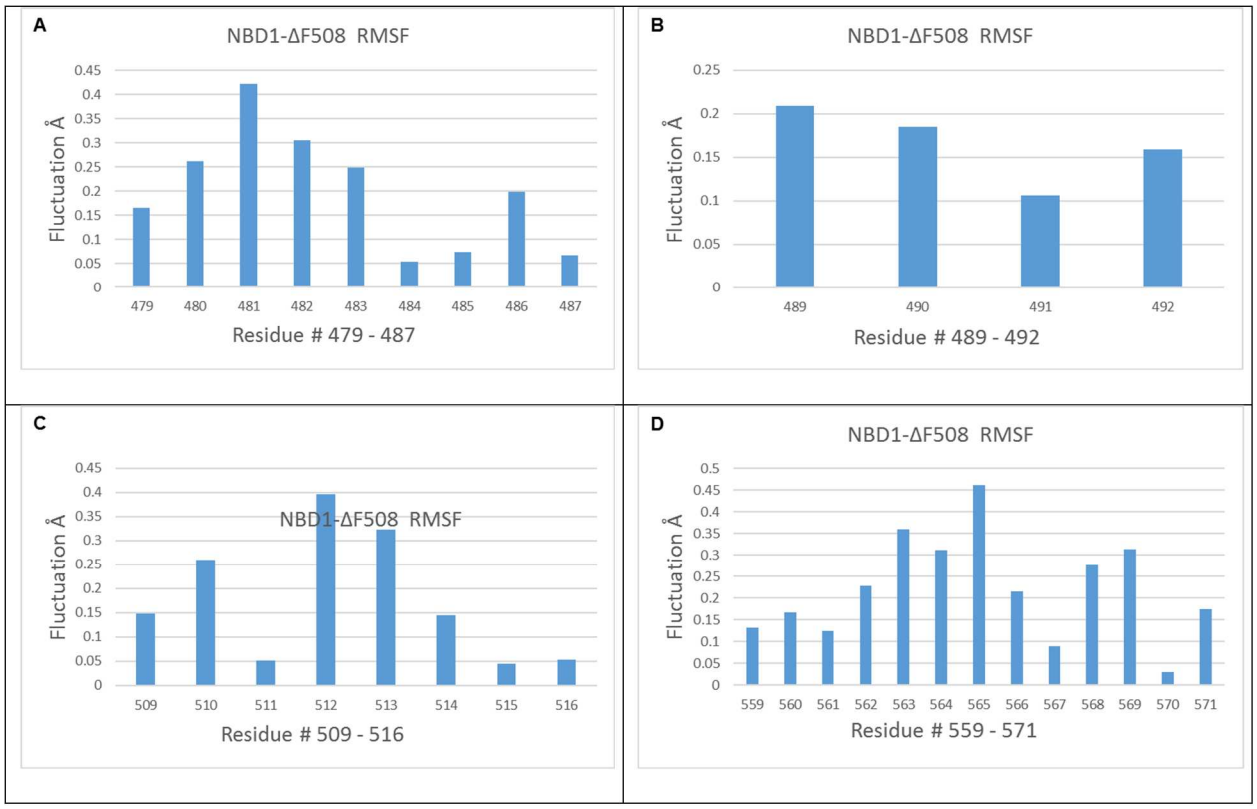

Figure 6: NBD1-ΔF508 RMSF of increased fluctuation.

A) RMSF of Residues 479 to 487. B) RMSF of Residues 489 to 492. C) RMSF of Residues from 509 to 516. D) RMSF of Residues 559 to 571.

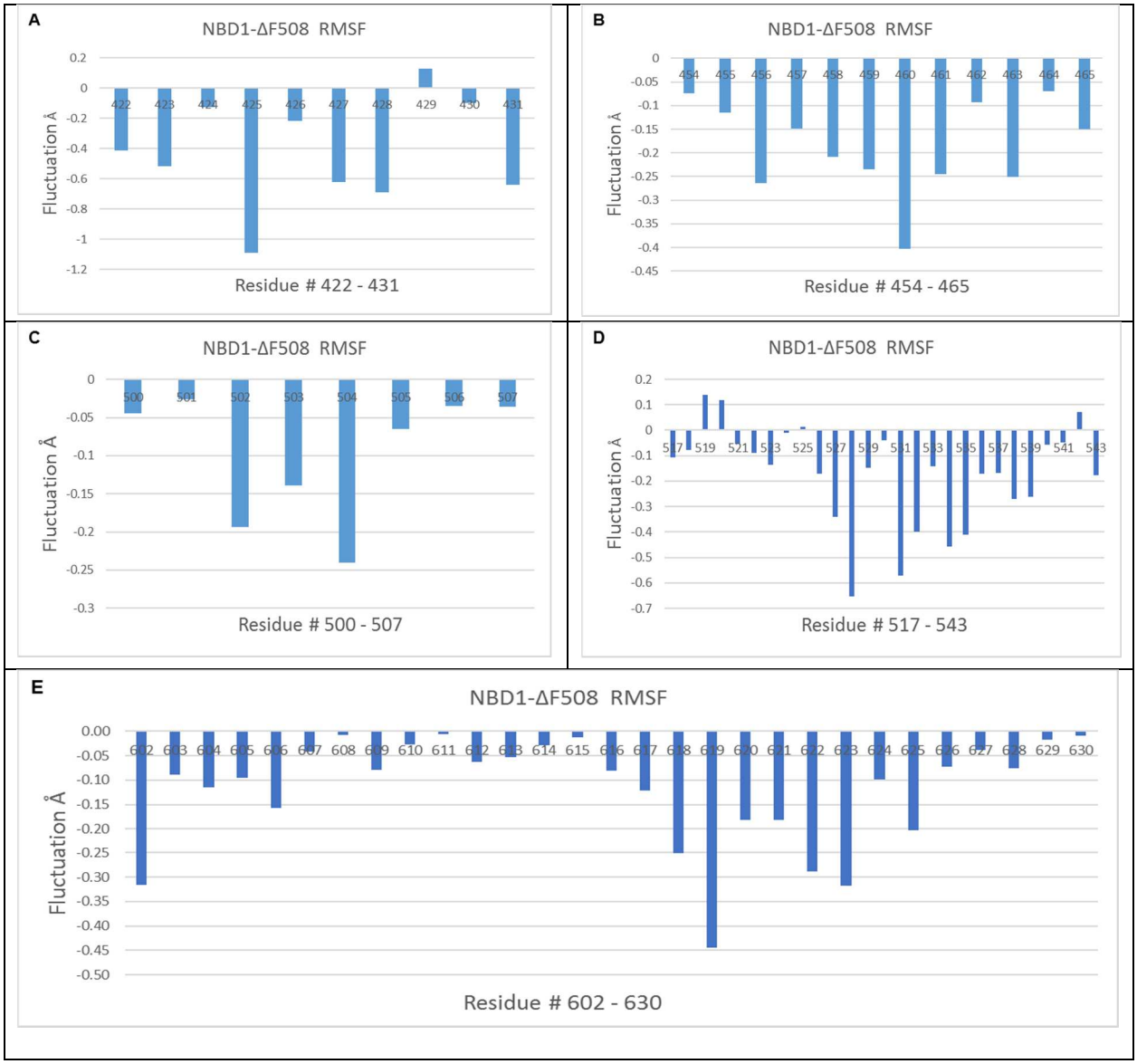

Figure 7: NBD1-ΔF508 RMSF of reduced fluctuation.

A) RMSF of Residues 422 to 431. B) RMSF of Residues 454 to 465. C) RMSF of Residues from 500 to 507. D) RMSF of Residues 517 to 543. E) RMSF of Residues of 602 to 630.

Purification of 6xHIS-SUMO-NBD1-ΔF508

Purification of NBD1 was attempted for use in DSF assays. In order for NBD1 to be soluble in aqueous solutions a SUMO-His tag was attached to NBD1 for an approximate size of 50 kDa. Figure 8 represents the results of the mouse NBD1 (NBD1) purification. The non-purified fractions (L2-L4) would display too much protein to identify the NBD1. The L5 fraction started the wash steps and showed increased resolution of protein bands, however, NBD1 could not yet be identified in these fractions without western blotting. The second wash step had little to no protein. The third wash step and nickel resin had similar appearances with a strong band at 50 kDa and traces amount of protein bands; however, both fractions contained more impurities than the eluted fraction. The elution step had a fainter protein band at the expected 50 kDa size with virtually no other bands present.

To confirm that the protein band at 50kDa was NBD1 a western blot was performed, displayed in Figure 9. The non-purified fractions (L2-L4) contained modest levels of NBD1.The two wash steps had little to no NBD1 (Fig 8 lane 5 and 6 vs. 7). The third wash step had a strong band which was comparable in size and intensity of the eluted protein band. There was a faint but clear His-positive band in the eluted fraction similar to the protein that remained on the nickel resin. This implied that a lot of the protein was either being washed off in the third wash step or remained bound on the nickel resin, possibly as aggregates.

A portion of the Elution fraction was used to determine protein concentration by gel densitometry with BSA as a reference. The gel of BSA and NBD1 showed strong bands in all lanes (Figure 10). It was observed that the BSA protein bands increased in intensity and contrast in direct relation to increased protein concentration. Concentration of the purified NBD1 was calculated by finding the linear regression of the plot of BSA concentration versus signal intensity obtained from the Gel Doc EZ gel software. The regression fit from the BSA plot was y=2.02E-008x + 0.0159. The R^2= 0.997 showed a strong correlation of the BSA concentration

with the signal intensity. This was used to calculate the concentration of the NBD1 samples at different volumes loaded on the gel (5µl, 10 µl, and 15 µl). The average concentration of NBD1 was calculated at 0.0697 mg/ml with a coefficient of variance of 2.00% (Table 2).

In the post elution fraction (Figure 11) there was inefficient cutting of the Smt3H tag. Two protein bands, one at the 50kb (6xhis-SUMO-NBD1-ΔF508) and the other between 25kb and 37kb, denoted incomplete cleavage activity. The SUMO His tag protease had incubated at 4^0C overnight which was at the lower end of reported activity range of 2^0C, however, the extended time was designed to allow time for cleavage most protein go happen under these conditions. Limited cleavage combined with the presence of a lot of protein in the nickel resin fraction after use of 400mM imidazole elution suggested protein aggregation (Rosen et al. 2002).

The 6xhis-SUMO-NBD1-ΔF508 concentration of 0.0697 mg/ml was lower than the expected value range of 0.2-0.5 mg/ml. Since the minimum protein concentration required to perform DSF was measured at 0.1 mg/ml, the purification could not be used for DSF experiments. The laboratory of Phillip J. Thomas provided a small quantity of purified mouse NBD1-ΔF508 (residue 389-673) for a limited number of DSF experiments (Figure 12).

Thermal Stability Measurements of NBD1

Two control ligands (ATP and BIA) were used to test the level of thermal stability of NBD1-ΔF508. ATP was used at 1 mM and 5 mM to determine a viable range of increased thermal stability (Table 3). ATP at 1 mM was observed to increase the melting temperature of NBD1-ΔF508 on average by $+3.73^0$C. The 5 mM ATP average concentration increased NBD1-ΔF508 by $+5.93^0$C. The calculated p-values ($p_{1\ mM\ ATP}$=0.00275, $p_{5\ mM\ ATP}$=0.00006) and F-critical values were lower than F-values ($F_{1\ mM\ ATP}$=43.40, $F_{5\ mM\ ATP}$=302.88, $F_{critical}$=7.709), combined with an acceptable variance of below 1^0C each ($variance_{1mM\ ATP}$=0.64, $variance_{5\ mM\ ATP}$=0.05),

suggesting the difference in melting temperature in the presence of the two ATP concentrations were statistically significant. While the trend of increased thermal stability were similar to a previous study, the results were modest compared to the 7^0C increase at 1 mM ATP (Sampson et al. 2011). In addition,1 mM BIA also increased NBD1's thermal stability (+2.13^{0}C). The calculated p-value for the 1 mM BIA data was statistically significant, and the F-value was higher compared to the F-critical ($p_{1\ mM\ BIA}$=0.03006, $F_{1\ mM\ BIA}$=10.86 $F_{critical}$=7.709). The $variance_{1mM\ BIA}$ was observed at 0.16 which demonstrated low dispersal of data. NBD1-ΔF508 was incubated with both ATP (1.5 mM) and BIA (1 mM) to determine if their effects are synergistic, or not. The multiple ligands increased thermal stability by 5.67^{0}C and was statistically significant ($p_{1.5\ mM\ ATP\ 1\ mM\ BIA}$=0.00015, $F_{1.5\ mM\ ATP\ 1\ mM\ BIA}$=194.59, $F_{critical}$=7.709) with low data dispersal (variance=0.21). This result suggests that multiple ligands combined can provide a synergistic effect on thermal stability.

The antioxidant Oleuropein is present in high concentrations in the olive plant and is known to prevent the aggregation of α-synuclein (Javed et al. 2019; Palazzi et al. 2018). In addition, Oleuropein can prevent the aggregation of NBD1-ΔF508 (residue 389-673) *in vitro* by ~40% (Youker Lab, Unpublished data). Therefore, Oleuropein and Hydroxy-tryosol (a metabolite of Oleuropein) were tested to determine if these compounds could increase NBD1-ΔF508 thermal stability. Oleuropein increased thermal stability by +0.26^{0}C, however, it was not deemed statistically significant due to the high p-value ($p_{Oleuropein}$=0.61671) and a F-value lower than F-critical $F_{Oleuropein}$=0.21, $F_{critical}$=7.709). Each concentration of Hydroxy-tyrosol tested had no positive effect on NBD1-ΔF508 thermal stability ($Tm_{100\ uM\ OH\text{-}Tyroso}$= -0.14^{0}C, $Tm_{500\ uM\ OH\text{-}Tyrosol}$= -0.24^{0}C, $Tm_{1\ mM\ OH\text{-}Tyrosol}$= -0.50^{0}C). The p-value for each concentration was high ($p_{100\ uM\ OH\text{-}Tyrosol}$=0.79986, $p_{500\ uM\ OH\text{-}Tyrosol}$=0.59343, $p_{1\ mM\ OH\text{-}Tyrosol}$=0.40977) and the F-values were low compared to F-critical($F_{100\ uM\ OH\text{-}Tyrosol}$= 0.07, $F_{500\ uM\ OH\text{-}Tyrosol}$=0.34, $F_{1\ mM\ OH\text{-}Tyrosol}$=0.85, $F_{critical}$=7.709), therefore the results were not statistically significant. When 1 mM Hydoxy-tyrosol

was combined with 1 mM BIA, the thermal stability increased, but the results were lower than 1 mM BIA only ($Tm_{1mM\ OH\text{-}Tyrosol\ 1\ mM\ BIA}$= +1.56^{0}C) suggesting an antagonist effect exerted by Hydoxy-tyrosol. This value was deemed significant with a low p-value ($p_{1\ mM\ OH\text{-}Tyrosol\ 1\ mM\ BIA}$=0.02076) and higher F-value compare to F-value($F_{1\ mM\ OH\text{-}Tyrosol\ 1\ mM\ BIA}$=13.72, $F_{critical}$=7.709). Data dispersal were low with $Variance_{1\ mM\ OH\text{-}Tyrosol\ 1\ mM\ BIA}$=0.21.

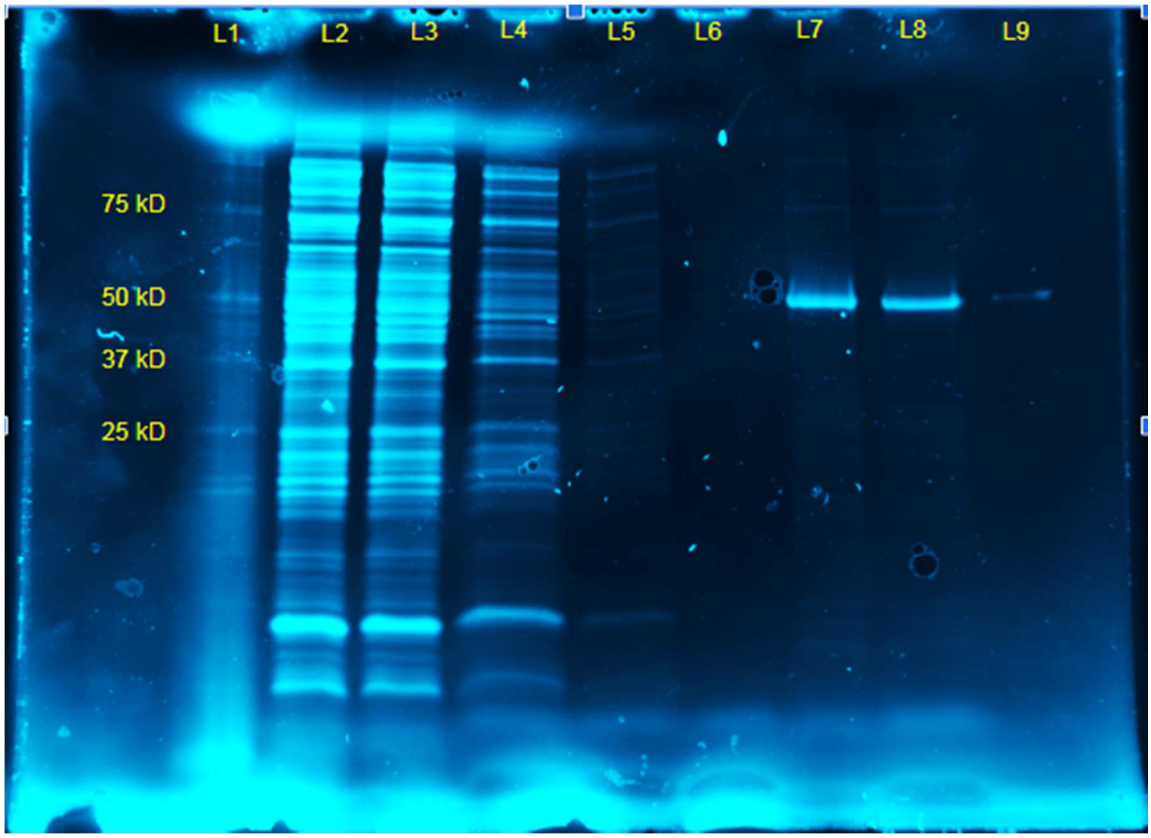

Figure 8:Stain Free Gel of CFTR NBD1 Purification steps.

A 250kb protein ladder (L1) was loaded to identify protein size. The Post-induction, Chemical lysis, and the Flow through (L2, L3, and L4) were added along with Wash steps 1, 2, and 3 (L5, L6, and L7) in the order of purification protocol order. The Ni-Resin, post wash step, were added in L8 and the Elution step in L9.

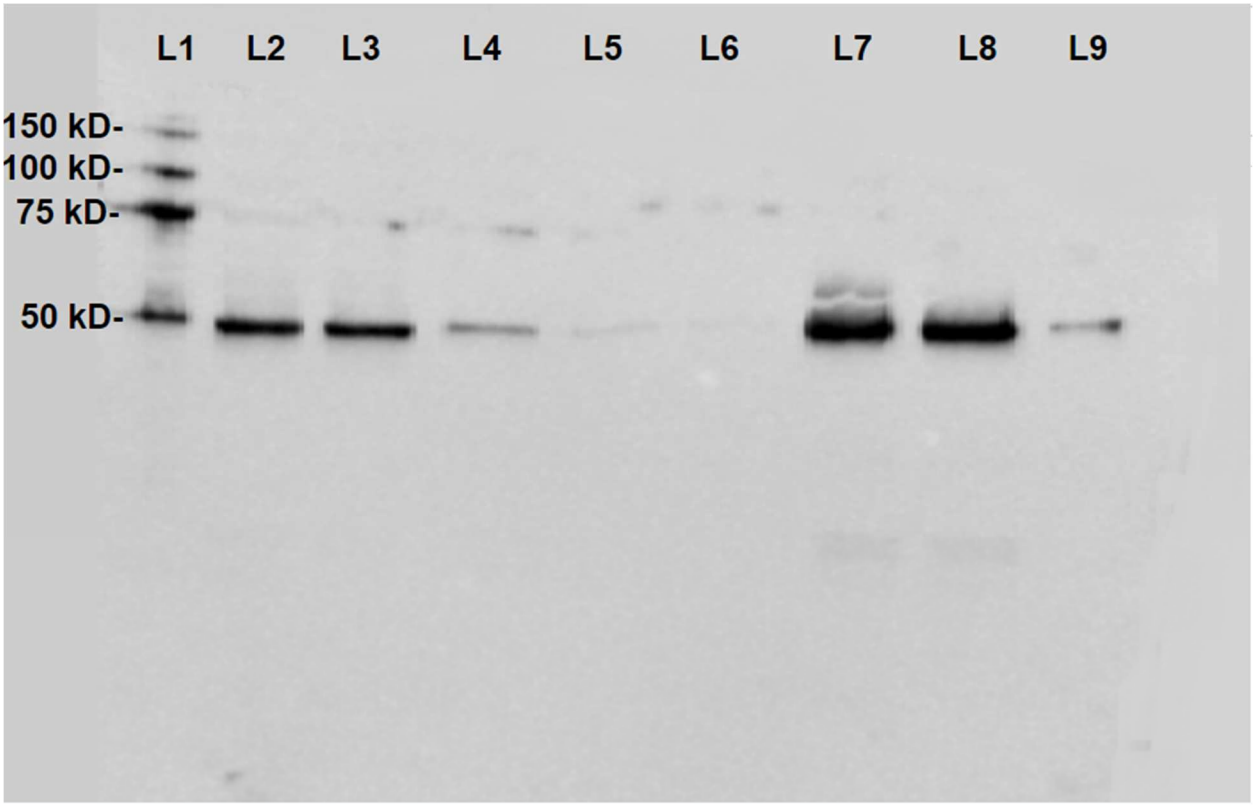

Figure 9:Western blot of 6xHis-SUMO-CFTR NBD1-Δ508

Sample lanes transferred from the Stain Free Gel and treated with 6x-His tag antibody. Lanes were identical to Stain Free Gel with 250kb protein ladder as L1. The Pre-chemical lysis, Chemical Lysis, and Flow through steps were labeled (L2, L3, and L4) respectively. L5-L7 represented wash step 1, 2, and 3. The Nickel resin appeared in L8 and Final elution in L9.

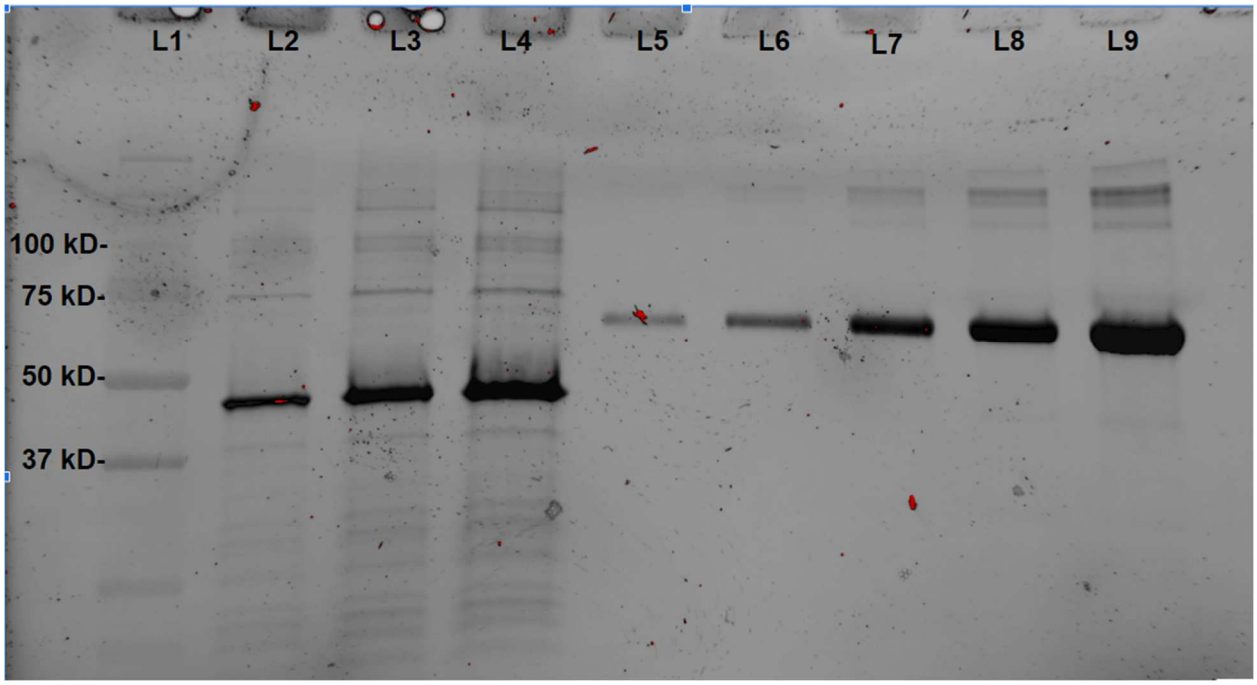

Figure 10:Stain Free Gel of BSA and 6xHIS-SUMO-ΔNBD1-508.

Three different NBD1 volumes (5 µl, 10 µl, and 15 µl) were loaded L2-L4. 10 µl of BSA were loaded at progressively higher concentrations (0.1 mg/ml, 0.2 mg/ml, 0.5 mg/ml, 1.0 mg/ml and 2.0 mg/ml) onto the gel with 0.1 mg/ml BSA at L5 and ending with 2.0 mg/ml BSA at L9.

Group	BSA Regression Curve	R^2 value	
BSA Range(0.1mg/ml - 2.0mg/ml)	y=2.02E-008x + 0.0159	0.997	
6xHIS-SUMO-NBD1 volume (µl)	5	10	15
Sample Concentration ug	0.342	0.6956	1.0677
Concentration mg/ml	0.0684	0.06956	0.07118
Group	Average (mg/ml)	STDEV	CV%
NBD1	0.0697	0.0014	2.00%

Table 2: 6HIS-SUMO-NBD1-ΔF508 concentration derived from BSA regression curve
Three NBD1 volumes had concentrations at 5 µl, 10 µl, and 15 µl were determined and the average, standard deviation, and coefficient of variance calculated.

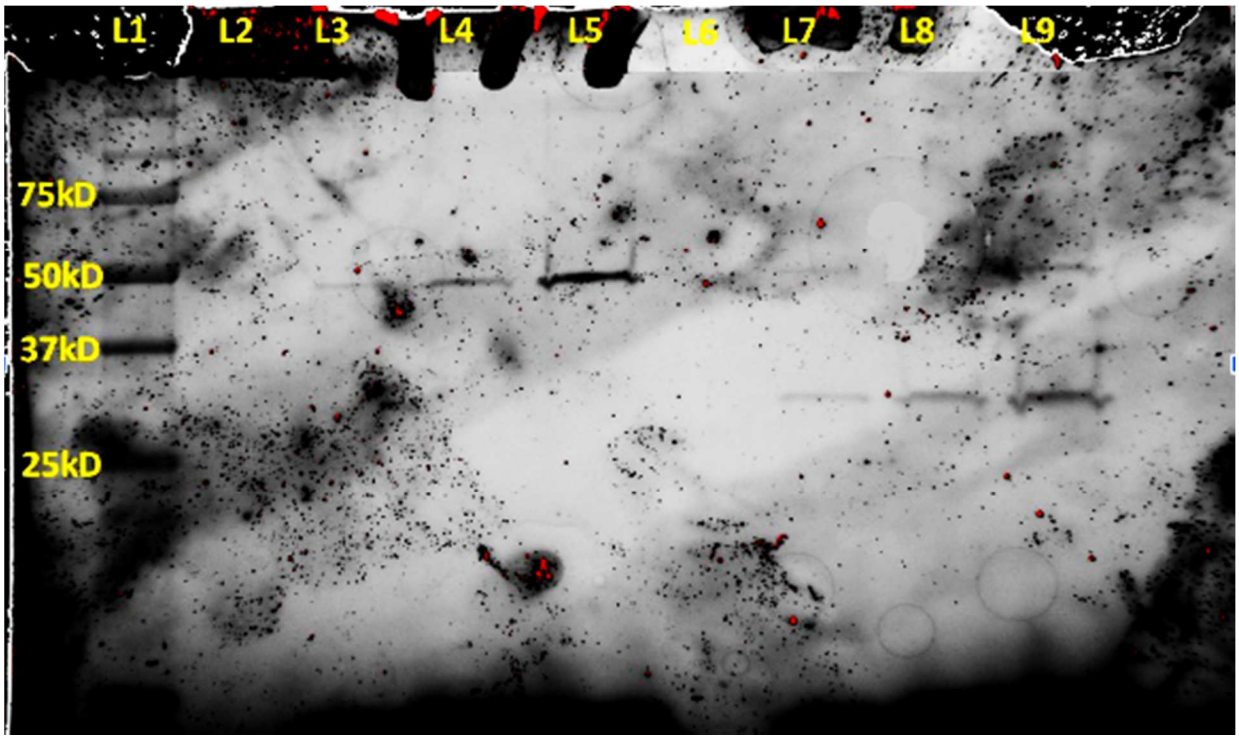

Figure 11: Stain Free Gel of non-cut vs cut Human CFTR-NBD1- ΔF508 dialyzed elution

A 250kb ladder (L1) was used to measure protein size. L3, L4, and L5 were the non-cut NBD1 protein at loading concentrations 5ul, 10ul, and 15ul respectively. The protease cut NBD1 were loaded with the same concentrations of L3-L5 in lanes L7-L9.

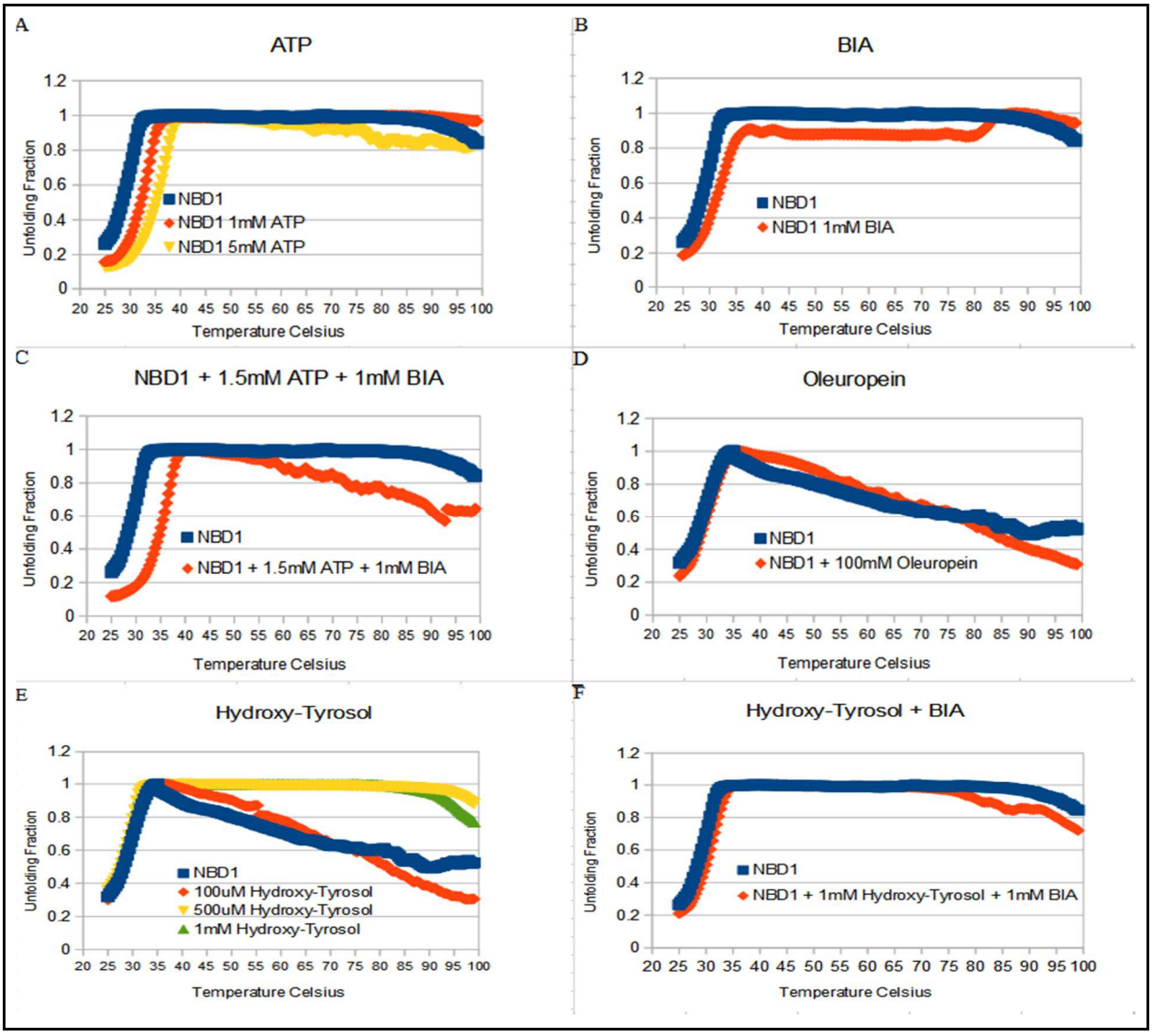

Figure 11:Representative DSF Melting Curves of NBD1-ΔF508

A) NBD1 in the presence of different concentrations of ATP. B) NBD1 with BIA. C) NBD1 with multi-ligand addition of ATP and BIA. D) NBD1 with Oleuropein. E) NBD1 with different concentrations of Hydroxy-Tyrosol. F) NBD1 with multi-ligand addition of BIA and Hydroxy-Tyrosol.

SUMMARY						
Groups	*Count*	*Sum*	*Average ^0C*	*Variance*		
NBD1	3	89.9	29.97	0.32		
NBD1 + 1mM ATP	3	101.1	33.70	0.64		
NBD1 + 5mM ATP	3	108.4	36.13	0.05		
NBD1 + 1mM BIA	3	96.3	32.10	0.16		
NBD1 + 1.5mM ATP + 1mM BIA	3	107.6	35.87	0.21		
NBD1 + 100uM Oleuropein	3	90.7	30.23	0.40		
NBD1 + 100uM Hydroxy-Tyrosol	3	89.5	29.83	0.40		
NBD1 + 500uM Hydroxy-Tyrosol	3	89.2	29.73	0.16		
NBD1 + 1mM Hydroxy-Tyrosol	3	88.4	29.47	0.56		
NBD1 + 1mM Hydroxy-Tyrosol + 1mM BIA	3	94.6	31.53	0.21		
ANOVA						
NBD1 vs Name	*SS*	*df*	*MS*	*F*	*P-value*	*F crit*
NBD1 + 1mM ATP	20.91	1	20.91	43.40	0.00275	7.709
NBD1 + 5mM ATP	57.04	1	57.04	302.88	0.00006	7.709
NBD1 + 1mM BIA	7.04	1	7.04	10.86	0.03006	7.709
NBD1 + 1.5mM ATP + 1mM BIA	52.21	1	52.21	194.59	0.00015	7.709
NBD1 + 100µM Oleuropein	0.11	1	0.11	0.29	0.61671	7.709
NBD1 + 100µM Hydroxy-Tyrosol	0.03	1	0.03	0.07	0.79986	7.709
NBD1 + 500µM Hydroxy-Tyrosol	0.08	1	0.08	0.34	0.59343	7.709
NBD1 + 1mM Hydroxy-Tyrosol	0.38	1	0.38	0.85	0.40977	7.709
NBD1 + 1mM Hydroxy-Tyrosol + 1mM BIA	3.68	1	3.68	13.72	0.02076	7.709

Table 3:One-Way ANOVA of NBD1-ΔF508 thermal stability with/without ligands.

The ANOVA displays the source of variation between NBD1-ΔF508 and each single group for the DSF Experimental results.

Discussion

The use of computational analysis of molecules through Molecular Dynamics serves to help screen for potential ligands for medical purposes. MD docking provided likely interactions of ligands to CFTR-NBD1ΔF508. Both visual and computational data predicted that BIA will bind near the same location as reported in the crystal structures in previous studies (Hall et al. 2016; He et al. 2015). Oleuropein had binding affinities comparable to BIA, however, the visual display had Oleuropein binding at the NBD1-ATP-NBD2 interface and thus not useful for increasing thermal stability of CFTR. Operating NAMD provided a general all-purpose MD simulation program that provides a quick analysis; however, the program does have its limitations. Simulations of 10ns were difficult to process in VMD. While the results are overall accurate, there are conflicting results such as V510 variability. NAMD predicted an increase in fluctuation while a previous study used Gromacs Molecular Dynamic software reported decreased fluctuations for the V510 residue (Zhenin, Noy, and Senderowitz 2015). MD simulation programs are numerous and evolving to create more accurate results. With purification difficulties of NBD1, MD is needed for efficient use of resources.

The purification of 6xHIS-SUMO-NBD1-ΔF508 yielded only trace amounts of protein. The literature stated that a concentration of 0.2- 0.5 mg concentration per liter culture can be achieved (Duffieux et al. 2000). The purification protocol utilized originally had a concentration of 60 mM Imidazole in the purification buffers. This high concentration was reduced to 20 mM Imidazole to reduce loss of NBD1 during the wash steps. The amount of NBD1 protein lost in wash step 1 and 2 were minimized, however, 6xhis-SUMO-NBD1-ΔF508 aggregated on the final wash step and nickel resin since a 400 mM imidazole elution failed to remove a large amount of 6xHIS-SUMO-NBD1-ΔF508. The purpose of purification of NBD1 at temperatures 16^0C and below was to allow for the protein to fold properly when expressed by the BL21 cell cultures and remain stable throughout the whole process. The Schmidt protocol lacked the cell

culture volume information and several buffer components were missing. The use of PMSF, NP40, and Lysozyme were researched and added to the protocol. These components were later confirmed by Phillip J. Thomas laboratory to be part of their NBD1 purification (personal communication). While this improved the elution concentration, the amount was still too low for DSF experiments. Future purification attempts could be improved by testing a filtration before the wash steps as NBD1 could be forming aggregates during the pre-wash steps and are precipitating on the nickel resin.

Another portion of the protocol that could be investigated and improved was the dialysis step. Several attempts to transfer the protein to the storage solution resulted in a complete protein crash with a semipermeable cellulose membrane. This could be that osmotic pressure caused a faster than desired exchange of water since the salt and glycerol concentrations were higher in the elution solution than in the storage solution. Greater success was achieved with the dialysis tubing technique which limits the speed of exchange of water. Gel filtration would be a possible way to further control the exchange of solutes.

DSF experiments were performed using NBD1-ΔF508 sample donated from the Phillip J. Thomas laboratory (UT Southwestern). A limited supply of NBD1-ΔF508 allowed for only a few DSF experiments. ATP and BIA had been identified as ligands that can increase NBD1-ΔF508 thermal stability (He et al. 2015; Sampson et al. 2011). While the trend of increased stability remained for ATP and BIA, the scaled increase was different compared to past studies. Both previous and current DSF studies of NBD1-ΔF508 without ligand had a thermal stability of approximately 30^0C. In a previous study using DSF, 1 mM ATP had increased NBD1 by 7^0C. This was higher than the reported results of 3.73^0C in this study. An increase to 5 mM ATP in the current study still demonstrated a stability less than the previous 1 mM study concentration albeit the result was much closer. A study by Lihua He used Differential Scanning Calorimetry (DSC) which increased the melting temperature of NBD1 1.4^0C higher when 1.5 mM BIA was

added (He et al. 2015). This was less than the 2.13^{0}C observed by the DSF method used in this study. Other studies show that Deoxythymidine triphosphate and 7-methyl-GTP increased thermal unfolding of protein by 3.0-3.3^{0}C more than ATP (C. Wang et al. 2018).

The purpose of the DSF experiment was to demonstrate the possibility of using multiple ligands to improve the thermal stability of NBD1.The use of 1 mM of BIA and 1.5 mM ATP had a near match in increased thermal stability compared to 5 mM ATP alone. This suggests that multiple ligands could have an additive or synergistic effect on NBD1 thermal stability. Oleuropein and one of its metabolites Hydroxy-tyrosol, had been investigated as possible benefits to CF patients (Lampronti et al. 2013). Oleuropein seemed to provide a very minor increase to thermal stability, however, it was not deemed statistically significant. This result matches with the docking results. The docking of Oleuropein to NBD1 was located at NBD1-ATP interface with NBD2. Even though the ΔG of Oleuropein was negative with negative full fitness score and thus energetically favorable, the location would be predicted to be difficult for the Oleuropein to reach in a heterodimer state (Ramsbottom et al. 2018; Kidd et al. 2004). The Oleuropein derivative, Hydroxy-tyrosol, was tested since this compound was more readily absorbed in the human body (de Bock et al. 2013). The results of Hydroxy-tyrosol showed no increase in thermal stability. When Hydroxy-tyrosol was added to BIA, the results did not increase the thermal stability beyond what was achieved with BIA alone. There is also a possibility that it might be antagonistic to BIA's protective effect and NBD1-ΔF508 interactions based upon the data results, however, more testing would need to be done to confirm or refute this possibility. Oleuropein and Hydroxy-tyrosol provide antioxidative, antiantherogenic, anticarcinogenic, and anti-inflammatory effects (de Bock et al. 2013; Lampronti et al. 2013). Based on this limited study, the positive effects on CF patients would most likely be from the reasons stated above and not from increasing thermal stability, or as a result of reducing protein aggregation.

Based on the BIA and ATP ligand results, combining multiple ligands to improve thermal stability is possible and could be investigated further. BIA is not the only known compound to increase thermal stability. RDR1 and RDR3 had shown promise in stabilizing NBD1-ΔF508 and increasing CFTR-ΔF508 maturation in cells (Sampson et al. 2011). The major obstacle was that the concentration needed to achieve a reasonable stability increase was high and toxicity is a major concern in the pharmaceutical industry. It would be beneficial if combining multiple ligands at lower concentrations in a “chemical cocktail” were found since that could limit toxicity and negative side effects. Testing multiple combinations of compounds could prove an alternative to the one compound cure that previous studies investigated.

References

Baker, Jennifer M R, Rhea P Hudson, Voula Kanelis, Wing-Yiu Choy, Patrick H Thibodeau, Philip J Thomas, and Julie D Forman-Kay. 2007. “CFTR Regulatory Region Interacts with NBD1 Predominantly via Multiple Transient Helices.” *Nature Structural & Molecular Biology* 14 (8): 738–45. https://doi.org/10.1038/nsmb1278.

Beek, Josy ter, Albert Guskov, and Dirk Jan Slotboom. 2014. “Structural Diversity of ABC Transporters.” *The Journal of General Physiology* 143 (4): 419–35. https://doi.org/10.1085/jgp.201411164.

Biemans-Oldehinkel, Esther, Mark K. Doeven, and Bert Poolman. 2006. “ABC Transporter Architecture and Regulatory Roles of Accessory Domains.” *FEBS Letters* 580 (4): 1023–35. https://doi.org/10.1016/j.febslet.2005.11.079.

Bock, Martin de, Eric B. Thorstensen, José G. B. Derraik, Harold V. Henderson, Paul L. Hofman, and Wayne S. Cutfield. 2013. “Human Absorption and Metabolism of Oleuropein and Hydroxytyrosol Ingested as Olive (*Olea Europaea* L.) Leaf Extract.” *Molecular Nutrition & Food Research* 57 (11): 2079–85. https://doi.org/10.1002/mnfr.201200795.

Cai, Zhi-wei, Jia Liu, Hong-yu Li, and David N Sheppard. 2011. “Targeting F508del-CFTR to Develop Rational New Therapies for Cystic Fibrosis.” *Acta Pharmacologica Sinica* 32 (6): 693–701. https://doi.org/10.1038/aps.2011.71.

Dean, M. 2001. “The Human ATP-Binding Cassette (ABC) Transporter Superfamily.” *Genome Research* 11 (7): 1156–66. https://doi.org/10.1101/gr.GR-1649R.

Djanic, M, N Pavlovic, B Stanimirov, T Stojancevic, S Golocorbin-Kon, G Bojic, and M Mikov. n.d. “Docking-Based Preliminary Study on the Interactions of Bile Acids with Drugs at the Transporter Level in Intestinal Bacteria,” 8.

Duffieux, Francis, Jean-Philippe Annereau, Julien Boucher, Emeric Miclet, Olivier Pamlard,

Michael Schneider, Véronique Stoven, and Jean-Yves Lallemand. 2000. “Nucleotide-Binding Domain 1 of Cystic Fibrosis Transmembrane Conductance Regulator: Production of a Suitable Protein for Structural Studies.” *European Journal of Biochemistry* 267 (17): 5306–12. https://doi.org/10.1046/j.1432-1327.2000.01614.x.

Grosdidier, A., V. Zoete, and O. Michielin. 2011. “SwissDock, a Protein-Small Molecule Docking Web Service Based on EADock DSS.” *Nucleic Acids Research* 39 (suppl): W270–77. https://doi.org/10.1093/nar/gkr366.

Hall, Justin D., Hong Wang, Laura J. Byrnes, Suman Shanker, Kelong Wang, Ivan V. Efremov, P. Andrew Chong, Julie D. Forman-Kay, and Ann E. Aulabaugh. 2016. “Binding Screen for Cystic Fibrosis Transmembrane Conductance Regulator Correctors Finds New Chemical Matter and Yields Insights into Cystic Fibrosis Therapeutic Strategy: CFTR Correctors in CF Therapeutics.” *Protein Science* 25 (2): 360–73. https://doi.org/10.1002/pro.2821.

He, Lihua, Andrei A. Aleksandrov, Jianli An, Liying Cui, Zhengrong Yang, Christie G. Brouillette, and John R. Riordan. 2015. “Restoration of NBD1 Thermal Stability Is Necessary and Sufficient to Correct ΔF508 CFTR Folding and Assembly.” *Journal of Molecular Biology* 427 (1): 106–20. https://doi.org/10.1016/j.jmb.2014.07.026.

Howell, L Daniel, Roy Borchardt, Jolanta Kole, Andrew M Kaz, Christoph Randak, and Jonathan A Cohn. 2004. “Protein Kinase A Regulates ATP Hydrolysis and Dimerization by a CFTR (Cystic Fibrosis Transmembrane Conductance Regulator) Domain.” *Biochemical Journal* 378 (Pt 1): 151–59. https://doi.org/10.1042/BJ20021428.

Humphrey, W., A. Dalke, and K. Schulten. 1996. “VMD: Visual Molecular Dynamics.” *Journal of Molecular Graphics* 14 (1): 33–38, 27–28. https://doi.org/10.1016/0263-7855(96)00018-5.

Hunt, J. F., C. Wang, and R. C. Ford. 2013. “Cystic Fibrosis Transmembrane Conductance Regulator (ABCC7) Structure.” *Cold Spring Harbor Perspectives in Medicine* 3 (2):

a009514–a009514. https://doi.org/10.1101/cshperspect.a009514.

Hwang, Tzyh-Chang, and David N. Sheppard. 2009. “Gating of the CFTR Cl ⁻ Channel by ATP-Driven Nucleotide-Binding Domain Dimerisation: CFTR Channel Gating.” *The Journal of Physiology* 587 (10): 2151–61. https://doi.org/10.1113/jphysiol.2009.171595.

Javed, Hayate, Mohamed Fizur Nagoor Meeran, Sheikh Azimullah, Abdu Adem, Bassem Sadek, and Shreesh Kumar Ojha. 2019. “Plant Extracts and Phytochemicals Targeting α-Synuclein Aggregation in Parkinson’s Disease Models.” *Frontiers in Pharmacology* 9 (March). https://doi.org/10.3389/fphar.2018.01555.

Jones, P. M., and A. M. George. 2002. “Mechanism of ABC Transporters: A Molecular Dynamics Simulation of a Well Characterized Nucleotide-Binding Subunit.” *Proceedings of the National Academy of Sciences* 99 (20): 12639–44. https://doi.org/10.1073/pnas.152439599.

Kidd, J. F., M. Ramjeesingh, F. Stratford, L.-J. Huan, and C. E. Bear. 2004. “A Heteromeric Complex of the Two Nucleotide Binding Domains of Cystic Fibrosis Transmembrane Conductance Regulator (CFTR) Mediates ATPase Activity.” *Journal of Biological Chemistry* 279 (40): 41664–69. https://doi.org/10.1074/jbc.M407666200.

Kolluru, Srikanth, Rosemary Momoh, Lydia Lin, Jayapal Reddy Mallareddy, and John L. Krstenansky. 2019. “Identification of Potential Binding Pocket on Viral Oncoprotein HPV16 E6: A Promising Anti-Cancer Target for Small Molecule Drug Discovery.” *BMC Molecular and Cell Biology* 20 (1). https://doi.org/10.1186/s12860-019-0214-3.

Kopito, Ron R. 1999. “Biosynthesis and Degradation of CFTR.” *Physiological Reviews* 79 (1): S167–73. https://doi.org/10.1152/physrev.1999.79.1.S167.

Lampronti, Ilaria, Monica Borgatti, Silvia Vertuani, Stefano Manfredini, and Roberto Gambari. 2013. “Modulation of the Expression of the Proinflammatory IL-8 Gene in Cystic Fibrosis Cells by Extracts Deriving from Olive Mill Waste Water.” *Evidence-Based Complementary and Alternative Medicine : ECAM* 2013.

https://doi.org/10.1155/2013/960603.

Lewis, H.A., C. Wang, X. Zhao, Y. Hamuro, K. Conners, M.C. Kearins, F. Lu, et al. 2010. “Structure and Dynamics of NBD1 from CFTR Characterized Using Crystallography and Hydrogen/Deuterium Exchange Mass Spectrometry.” *Journal of Molecular Biology* 396 (2): 406–30. https://doi.org/10.1016/j.jmb.2009.11.051.

Lewis, Hal A, Sean G Buchanan, Stephen K Burley, Kris Conners, Mark Dickey, Michael Dorwart, Richard Fowler, et al. 2004. “Structure of Nucleotide-Binding Domain 1 of the Cystic Fibrosis Transmembrane Conductance Regulator.” *The EMBO Journal* 23 (2): 282–93. https://doi.org/10.1038/sj.emboj.7600040.

Li, Chunying, and Anjaparavanda P. Naren. 2011. “Analysis of CFTR Interactome in the Macromolecular Complexes.” In *Cystic Fibrosis*, edited by Margarida D. Amaral and Karl Kunzelmann, 741:255–70. Totowa, NJ: Humana Press. https://doi.org/10.1007/978-1-61779-117-8_17.

Luckie, Douglas, John Wilterding, Marija Krha, and Mauri Krouse. 2003. “CFTR and MDR: ABC Transporters with Homologous Structure but Divergent Function.” *Current Genomics* 4 (3): 225–35. https://doi.org/10.2174/1389202033490394.

Molinski, Steven, Paul D. W. Eckford, Stan Pasyk, Saumel Ahmadi, Stephanie Chin, and Christine E. Bear. 2012. “Functional Rescue of F508del-CFTR Using Small Molecule Correctors.” *Frontiers in Pharmacology* 3. https://doi.org/10.3389/fphar.2012.00160.

Palazzi, Luana, Elena Bruzzone, Giovanni Bisello, Manuela Leri, Massimo Stefani, Monica Bucciantini, and Patrizia Polverino de Laureto. 2018. “Oleuropein Aglycone Stabilizes the Monomeric α-Synuclein and Favours the Growth of Non-Toxic Aggregates.” *Scientific Reports* 8 (1). https://doi.org/10.1038/s41598-018-26645-5.

Patrick, Anna E. 2012. “Development of CFTR Structure.” *Frontiers in Pharmacology* 3. https://doi.org/10.3389/fphar.2012.00162.

Phillips, James C., Rosemary Braun, Wei Wang, James Gumbart, Emad Tajkhorshid, Elizabeth

Villa, Christophe Chipot, Robert D. Skeel, Laxmikant Kalé, and Klaus Schulten. 2005. “Scalable Molecular Dynamics with NAMD.” *Journal of Computational Chemistry* 26 (16): 1781–1802. https://doi.org/10.1002/jcc.20289.

Rabeh, Wael M., Florian Bossard, Haijin Xu, Tsukasa Okiyoneda, Miklos Bagdany, Cory M. Mulvihill, Kai Du, et al. 2012. “Correction of Both NBD1 Energetics and Domain Interface Is Required to Restore ΔF508 CFTR Folding and Function.” *Cell* 148 (1–2): 150–63. https://doi.org/10.1016/j.cell.2011.11.024.

Rosen, Ran, Dvora Biran, Eyal Gur, DÃ¶rte Becher, Michael Hecker, and Eliora Z. Ron. 2002. “Protein Aggregation in *Escherichia Coli* : Role of Proteases.” *FEMS Microbiology Letters* 207 (1): 9–12. https://doi.org/10.1111/j.1574-6968.2002.tb11020.x.

Sampson, Heidi M., Renaud Robert, Jie Liao, Elizabeth Matthes, Graeme W. Carlile, John W. Hanrahan, and David Y. Thomas. 2011. “Identification of a NBD1-Binding Pharmacological Chaperone That Corrects the Trafficking Defect of F508del-CFTR.” *Chemistry & Biology* 18 (2): 231–42. https://doi.org/10.1016/j.chembiol.2010.11.016.

Schmidt, André, Juan L. Mendoza, and Philip J. Thomas. 2011. “Biochemical and Biophysical Approaches to Probe CFTR Structure.” In *Cystic Fibrosis*, edited by Margarida D. Amaral and Karl Kunzelmann, 741:365–76. Totowa, NJ: Humana Press. https://doi.org/10.1007/978-1-61779-117-8_24.

Sorum, Ben, Dávid Czégé, and László Csanády. 2015. “Timing of CFTR Pore Opening and Structure of Its Transition State.” *Cell* 163 (3): 724–33. https://doi.org/10.1016/j.cell.2015.09.052.

Vasiliou, Vasilis, Konstandinos Vasiliou, and Daniel W Nebert. 2008. “Human ATP-Binding Cassette (ABC) Transporter Family.” *Human Genomics* 3 (3): 281. https://doi.org/10.1186/1479-7364-3-3-281.

Vela-Corcía, David, Diego Romero, Antonio de Vicente, and Alejandro Pérez-García. 2018. “Analysis of β-Tubulin-Carbendazim Interaction Reveals That Binding Site for MBC

Fungicides Does Not Include Residues Involved in Fungicide Resistance." *Scientific Reports* 8 (1). https://doi.org/10.1038/s41598-018-25336-5.

Walker, J E, M Saraste, M J Runswick, and N J Gay. 1982. "Distantly Related Sequences in the Alpha- and Beta-Subunits of ATP Synthase, Myosin, Kinases and Other ATP-Requiring Enzymes and a Common Nucleotide Binding Fold." *The EMBO Journal* 1 (8): 945–51.

Wang, C. K., S. K. Weeratunga, C. M. Pacheco, and A. Hofmann. 2012. "DMAN: A Java Tool for Analysis of Multi-Well Differential Scanning Fluorimetry Experiments." *Bioinformatics* 28 (3): 439–40. https://doi.org/10.1093/bioinformatics/btr664.

Wang, Chi, Andrei A. Aleksandrov, Zhengrong Yang, Farhad Forouhar, Elizabeth A. Proctor, Pradeep Kota, Jianli An, et al. 2018. "Ligand Binding to a Remote Site Thermodynamically Corrects the F508del Mutation in the Human Cystic Fibrosis Transmembrane Conductance Regulator." *Journal of Biological Chemistry* 293 (46): 17685–704. https://doi.org/10.1074/jbc.RA117.000819.

Wilkens, Stephan. 2015. "Structure and Mechanism of ABC Transporters." *F1000Prime Reports* 7 (February). https://doi.org/10.12703/P7-14.

Zhang, Zhe, and Jue Chen. 2016. "Atomic Structure of the Cystic Fibrosis Transmembrane Conductance Regulator." *Cell* 167 (6): 1586-1597.e9. https://doi.org/10.1016/j.cell.2016.11.014.

Zhenin, Michael, Efrat Noy, and Hanoch Senderowitz. 2015. "REMD Simulations Reveal the Dynamic Profile and Mechanism of Action of Deleterious, Rescuing, and Stabilizing Perturbations to NBD1 from CFTR." *Journal of Chemical Information and Modeling* 55 (11): 2349–64. https://doi.org/10.1021/acs.jcim.5b00312.

(C. K. Wang et al. 2012)